SAN-1250-2

RESEARCH ON LATTICE-MISMATCHED SEMICONDUCTOR LAYERS

Progress Report No. 2 for August 16, 1977—May 15, 1978

By
R. L. Moon

May 1978

Work Performed Under Contract No. EY-76-C-03-1250

Varian Associates, Inc.
Palo Alto, California

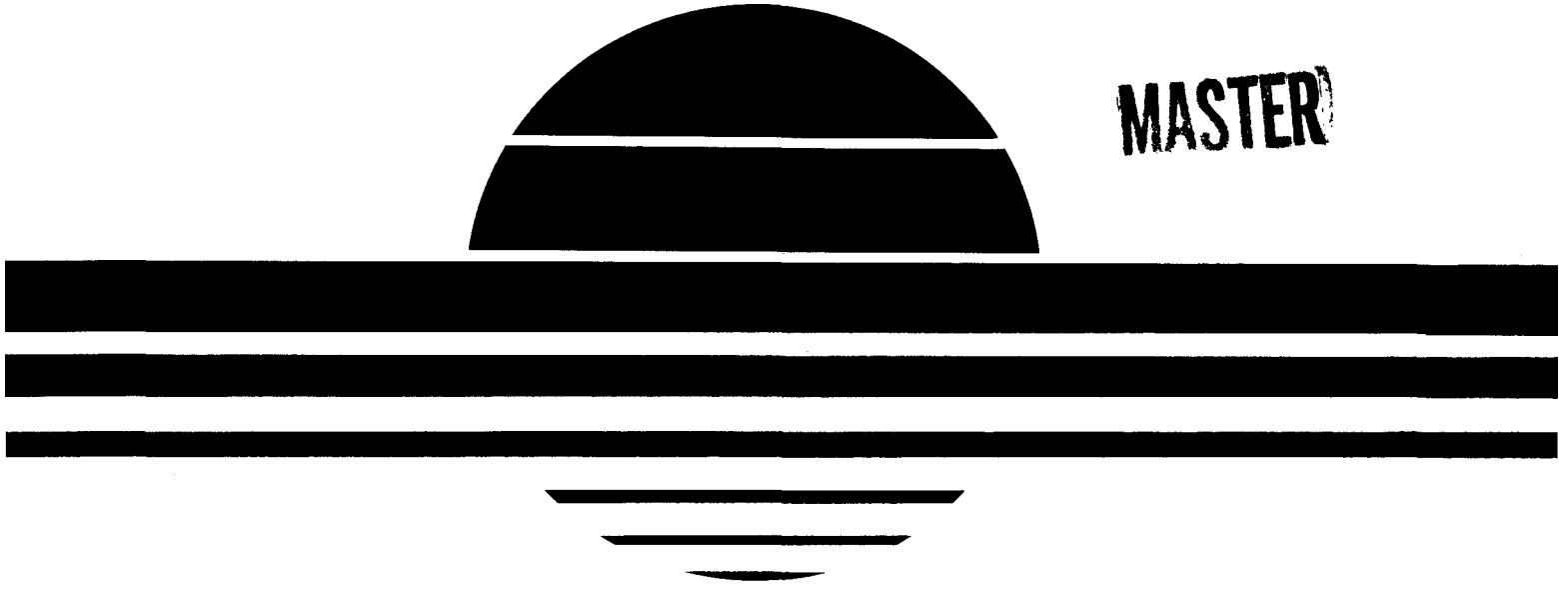

U.S. Department of Energy

Solar Energy

NOTICE

SAN-1250-2
Distribution Category UC-63

RESEARCH ON LATTICE-MISMATCHED SEMICONDUCTOR LAYERS

PROGRESS REPORT NO. 2

(16 Aug 1977 - 15 May 1978)

May 1978

Sponsored by

U.S. Energy and Development Administration
Washington, DC 20545

Contract No. EY-76-C-03-1250

* * *

Prepared by

R. L. Moon

Varian Associates, Inc.
611 Hansen Way
Palo Alto, CA 94303

SUMMARY

Investigations of the $Al_xGa_{1-x}As_{1-y}Sb_y$ quaternary alloy have shown that compositions necessary for a two-junction stacked solar cell can be grown by LPE. Aluminum concentrations of 88 mole% have been grown in an alloy containing 16 mole% Sb. For a constant Al concentration in the solution, the addition of Sb causes Al incorporation in the solid to decrease. Antimony behavior is similar to that observed in the GaAsSb ternary system.

Lattice constant grading using Al depletion to change As activity has been used to continuously grade from GaAs to $Al_{.01}Ga_{.99}As_{.84}Sb_{.16}$. Layers of $GaAs_{.84}Sb_{.16}$ have been routinely grown on the graded layer. The best orientation for combining good growth rate, surface morphology and solution removal has been the GaAs (111)A surface. Growth rates for the conditions used are in the order (100) > (111)A > (111)B. Superior layer morphology has been observed when the growth solution is Sb rich. A fine cross hatch pattern has been observed on continuously graded layers > 20 microns thick with a mismatch of 1.3%.

Etch-pit densities are normally $\geq 10^6$ cm^{-2} after grading and sometimes inhomogeneously distributed. Etch-pit studies during the early stages of growth suggest that dislocation bunching occurs at this stage. At high localized dislocation densities large slip-like bands have been observed.

Tin doping of GaAsSb is shown to be dependent upon which side of the pseudobinary growth occurs. The net electron concentration for a given X^{ℓ}_{Sn} is observed to be higher when growth is from an Sb-rich solution.

Complete 1.15-eV solar cells consisting of $Al_{.6}Ga_{.4}As_{.85}Sb_{.15}$/$GaAs_{.84}Sb_{.16}$/graded AlGaAsSb/GaAs(111)A have been fabricated and tested. The maximum quantum efficiency in the cells tested to date has been 25%; a value caused by diffusion lengths $\leq$ 0.5 micron. The reason for the low diffusion length is not clear and is under investigation. GaAsSb p-n junctions with low leakage currents over areas as large as 0.68 cm^2 have been grown on continuously graded layers. Good junction characteristics over such a large area indicate that inclusion problems sometimes associated with LPE grading can be eliminated.

TABLE OF CONTENTS

1. INTRODUCTION

It has been the purpose of this portion of the contract to investigate the AlGaAsSb quaternary system as a possible candidate for a two-junction high efficiency solar cell and to ascertain the associated materials problems. In this alloy system the lattice constant is primarily determined by the Sb/As ratio in the column-V sublattice, while at any given concentration of Sb in the solid, substitution of Al for Ga only serves to increase the bandgap. Cells can then be fabricated one upon the other at a given lattice constant. This is in practice an essential condition for success of the "monolithic" multilayer all-epitaxial approach to high efficiency cells.

Some appreciation of the uniformity demands in this scheme relative to most semiconductor devices can be obtained by simply comparing the area ratio of a solar cell to a mesa diode. The AlGaAs/GaAs concentration solar cell fabricated at Varian is 0.56 cm^2, while an average mesa diode may be $\sim 10^{-4}$ cm^2; an area ratio of $\sim$ 5000. Every characteristic of a grown wafer such as surface morphology, dislocation distribution, inclusion pattern, etc. has a direct bearing on the final performance. A selection of a few devices from several hundred on a wafer is no longer possible.

2. GENERAL CHARACTERISTICS OF THE AlGaAsSb QUATERNARY SYSTEM

The bandgap and lattice constant features of AlGaAsSb are summarized in Fig. 1 where their variations are shown as a function of concentration. Basically, lattice constant variations are seen to depend mainly on the Sb and As content in the column-V sublattices; near vertical isolattice constant lines result. Bandgap behavior is divided into a direct and indirect region as the ordering of the conduction bands changes. This transition occurs at Al concentrations between 30 and 50 at% depending on the Sb concentration. So at the higher Al concentrations the nature of AlGaAsSb is that of indirect optical absorption. Behavior is analogous to that of AlGaAs, with an additional component.

Not shown on this diagram is the often-discussed miscibility gap in the $GaAs_{1-x}Sb_x$ system which is believed to occur for at $0.38 < x < 0.61$ (Ref. 1). Estimates of the maximum temperature or critical temperature for occurence of the immiscibility region is ~ 730°C. Recently, two groups using MBE with substrates at 550°C[2] and 600°C[3] have succeeded in growing GaAsSb in the immiscibility range. These results coupled with much earlier results of Muller and Richards[4] using flash evaporation suggest that nucleation difficulties associated with LPE are responsible for the observed miscibility behavior.

Understanding much of the behavior in this system would be simplified if a complete phase diagram were available. Since this does not exist, a temporary expedient is to examine the trends shown in Fig. 2 for the GaAsSb ternary alloy phase field.[1] The data have been arranged as a function of the Sb/Ga weight ratio in solution to simplify comparison with experimental conditions. As can be seen, the same composition can be grown from both the column-III and column-V rich regions. Since VPE occurs with

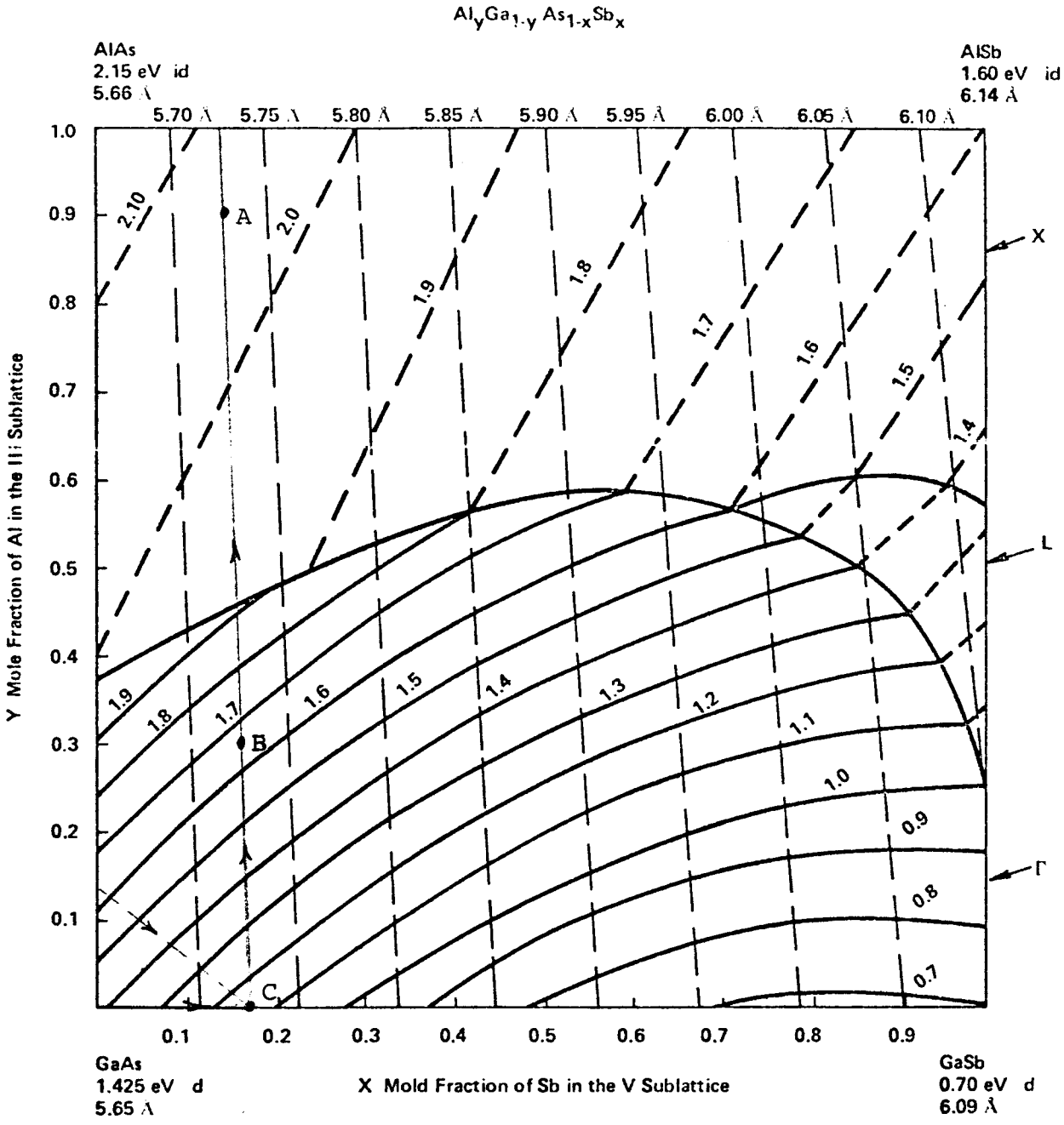

Fig. 1. Bandgap and lattice constant variations vs composition in the AlGaAsSb quaternary alloy system.

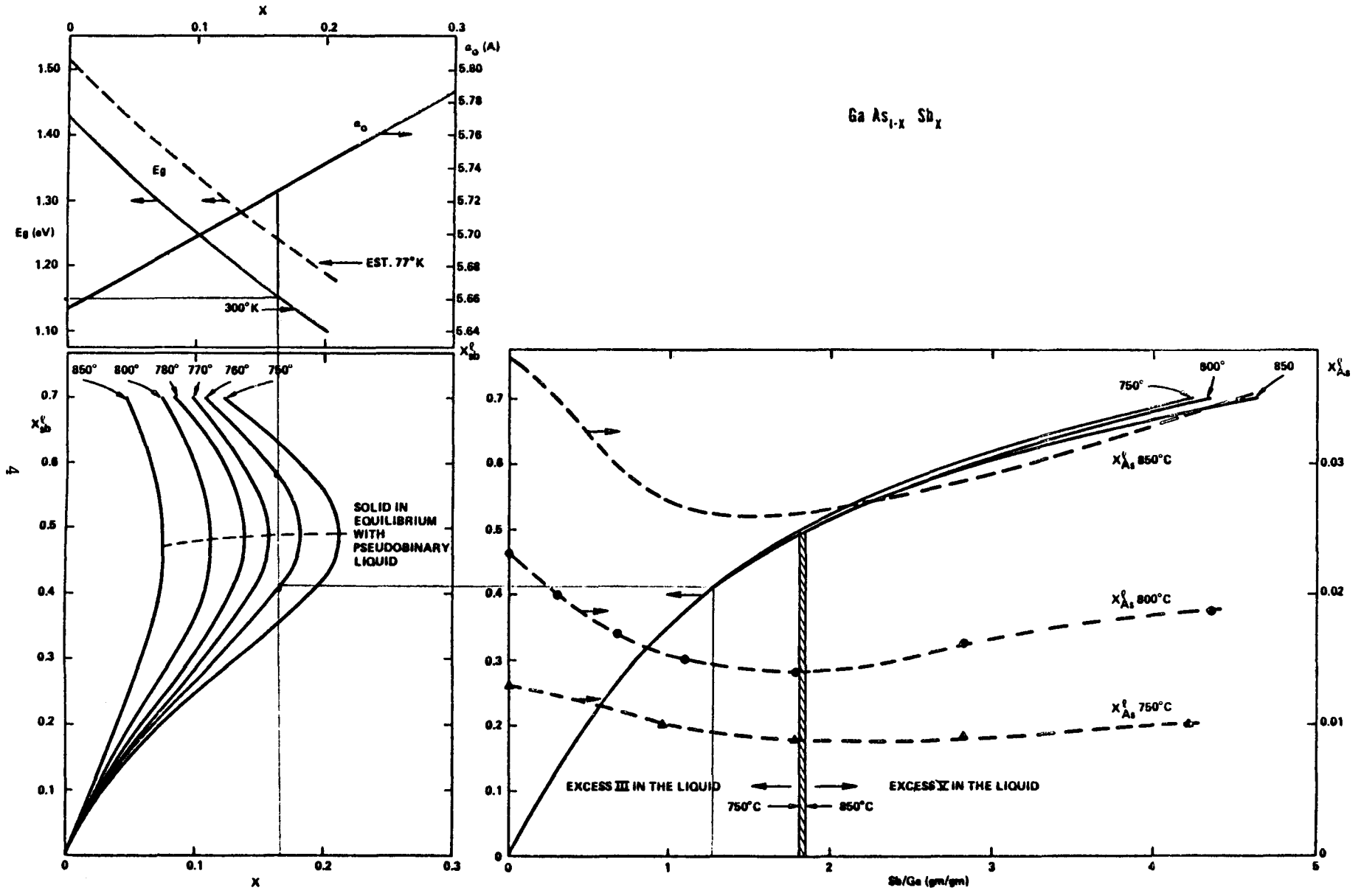

Fig. 2. Phase equilibrium data for the GaAsSb ternary system as a function of Sb/Ga weight ratio.

excess column-V present during deposition, defect densities characteristic of VPE should in principle be possible from a liquid solution environment. An example of the versatility of this system is demonstrated by examining the solution compositions which are capable of producing a 1.15-eV solid. The lines drawn on Fig. 2 show the procedure. Picking the bandgap at 1.15 eV, the vertical line intersects the 760°C isotherm of the X_{Sb}^{ℓ} vs X plot at two points, namely X_{Sb}^{ℓ} = 0.625 and 0.42 for X = 0.165. By drawing horizontal lines over to the right-hand portion of the figure, the X_{As}^{ℓ} and correct Sb/Ga ratios can be determined. Notice that X_{As}^{ℓ} passes through a minimum at the stoichiometric composition.

3. ALUMINUM AND Sb INCORPORATION

Previous work[4] at a Sb/Ga ratio = 0.3 has shown that increases in Al content in solution cause both a bandgap increase and a reduction in As solubility. Since the lattice parameter is nearly constant upon Al addition to the growth solution, the As segregation coefficient must increase. At the same time, Sb incorporation has been shown to be independent of Al concentration in solution. To extend the general survey of the AlGaAsSb alloy behavior to the compositional range of interest, the Al behavior has been examined as a function of Sb in solution at a constant X^{ℓ}_{Al} and as a function of Al concentration at constant X^{ℓ}_{Sb}. Aluminum incorporation in the solid AlGaAsSb alloy as a function of Al in solution is shown in Fig. 3 for a growth temperature of 785°C and X^{S}_{Sb} = 0.17. The high Al concentration values represent data from 12 samples. Values of Al in the solid of 88% correspond to an indirect bandgap of 2.05 eV. The transition between the direct and indirect region ($\Gamma \rightarrow X$ conduction band minima) occurs near $X^{S}(Al) = 0.48$ for an $X^{S}(Sb) = 0.17$. For comparison, Al incorporation into AlGaAs ($X^{\ell}_{Sb} = 0$) is also shown.

To confirm that addition of Sb in solution decreases the Al segregation coefficient data from a series of lattice constant grading runs have been analyzed; the results are seen in Fig. 4. In this figure the maximum Al and Sb concentrations have been determined from electron microprobe scans across cleaved sections of layers grown between 830 and 770°C at a cooling rate of 0.5°C/min. The maximum Al concentration occurred at the beginning of growth ~ 825°C while Sb reached its maximum at the end of growth, 770°C. The atomic fraction of Al in solution varied from 2.75 x 10^{-3} at Sb/Ga = 0.31 to 4 x 10^{-3} at Sb/Ga = 8. As can be seen, Al incorporation in the solid decreases as the solution becomes richer in Sb.

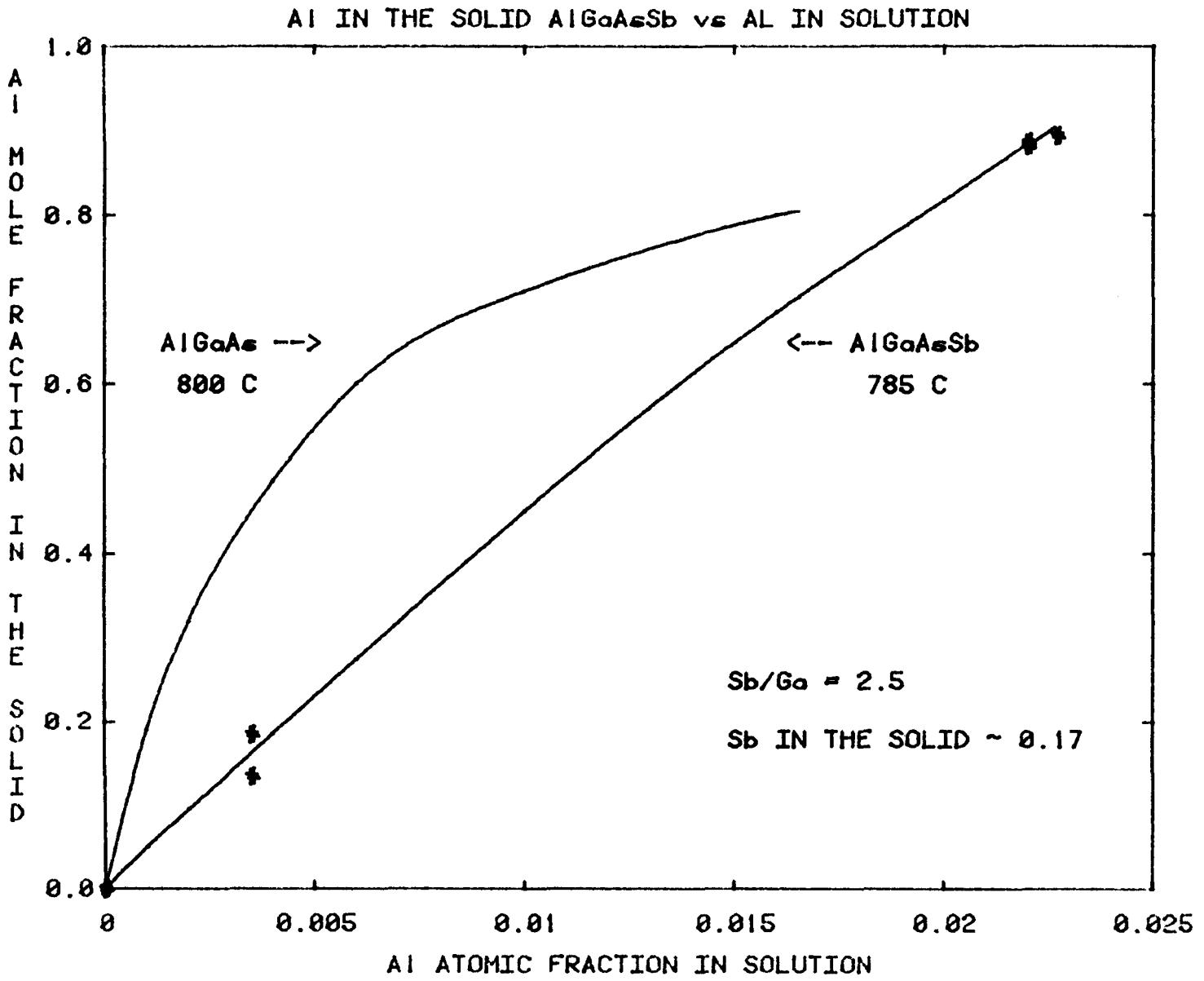

Fig. 3. Aluminum incorporation into AlGaAsSb as a function of Al concentration in solution.

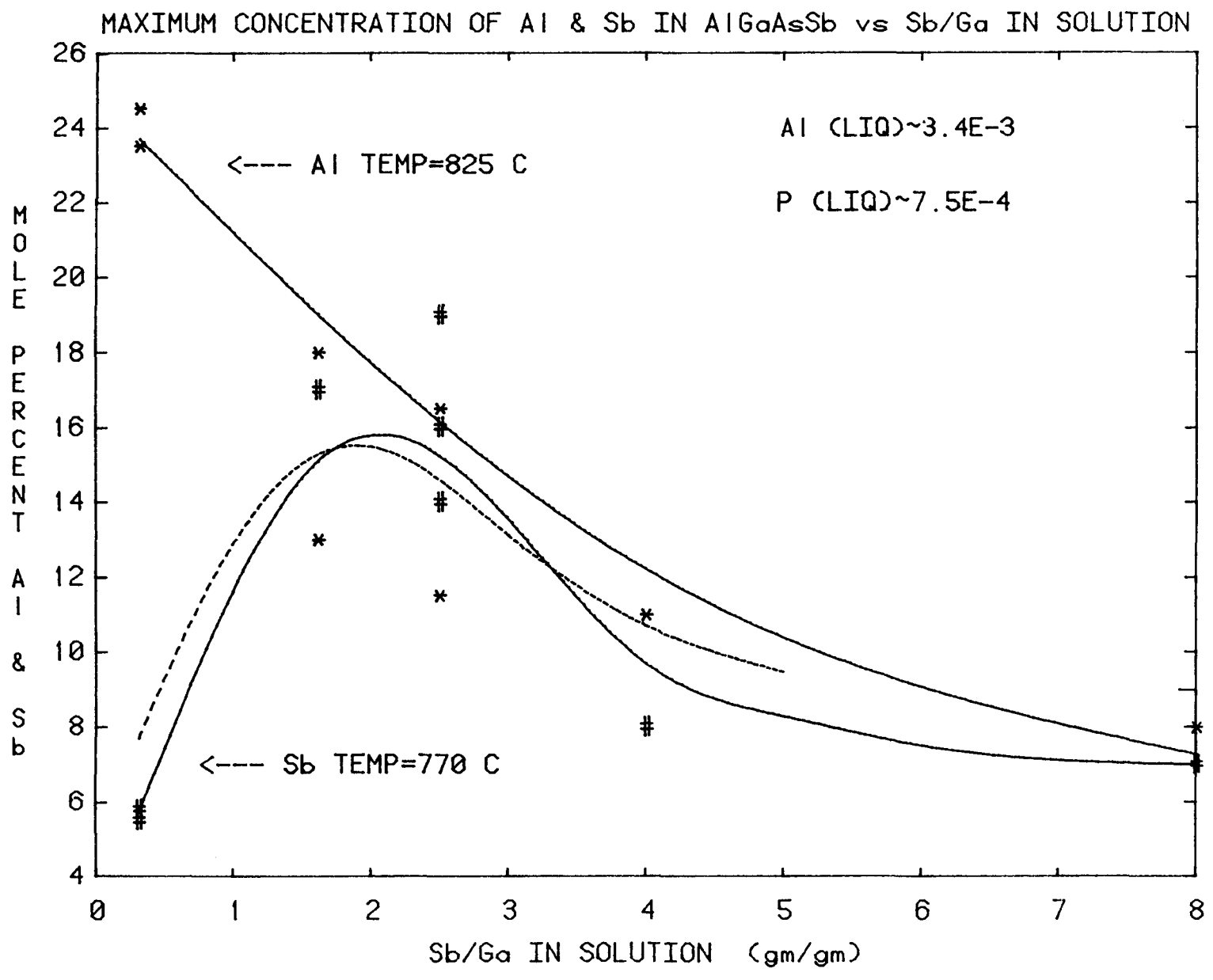

Fig. 4. Aluminum and Sb incorporation into AlGaAsSb as a function of Sb/Ga weight ratio.

Antimony, on the other hand, goes through a maximum at Sb/Ga ~ 1.8 (the pseudo binary boundary) and then decreases as the solution becomes richer in the column-V element. This trend is the same as that observed for a Ga-As-Sb system and the data for that system are included. Scatter in the experimental data prevents better comparison between Sb incorporation in the solid with and without Al in the solution.

An important point that remains to be investigated is whether small additions of Al to a Ga-As-Sb solution causes a decrease in lattice constant. Data are conflicting on this point.[4] At a growth temperature of 720°C a decrease was observed, but at 760°C it was not. This must be resolved if lattice matching, rather than just epitaxy, is to be accomplished.

4. LATTICE CONSTANT GRADING

Most of the work reported here has been performed on GaAs (111)A substrates because this orientation yields superior solution removal and surface morphology properties. Two types of grading have been investigated: continuous and step grading using either one solution or several solutions, respectively. In the continuous case, grading has been achieved using Al depletion to change As activity in an Al-Ga-As-Sb solution, while in step grading the solutions contained only Ga-As-Sb at different compositions to provide incremental changes in composition.

Lattice constant changes from 5.65 Å in the substrate to ~ 5.73 Å in the epitaxial layer have been investigated. Mismatch defined as $2(a_s-a_e)/(a_s+a_e)$, amounts to 1.3%. Within this mismatch range lies the compositions of interest for a two-junction monolithic solar cell. Maximum Sb concentration in $GaAs_{1-x}Sb_x$ is 16.5%.

4.1 Continuous and Step Grading

Cooling intervals for both methods have been normally between 830-770°C, a range required more for continuous grading where the presence of Al reduces As solubility. A typical concentration profile obtained by electron microprobe analysis across a cleaved section is shown in Fig. 5. Additional evidence of lattice constant grading is seen in Fig. 6 which shows a (444) diffractometer pattern of a GaAsSb/AlGaAsSb graded layer. Immediately evident is the gradual change in lattice constant from GaAs to GaAsSb

In order to establish the various solid concentrations as a function of temperature during continuous grading, the following experiment was performed: growth was initiated at 830°C from a solution with a ratio of Sb/Ga = 2.5 g/g and continued at a cooling rate of 0.14°C/min down to 770°C. At 12° intervals

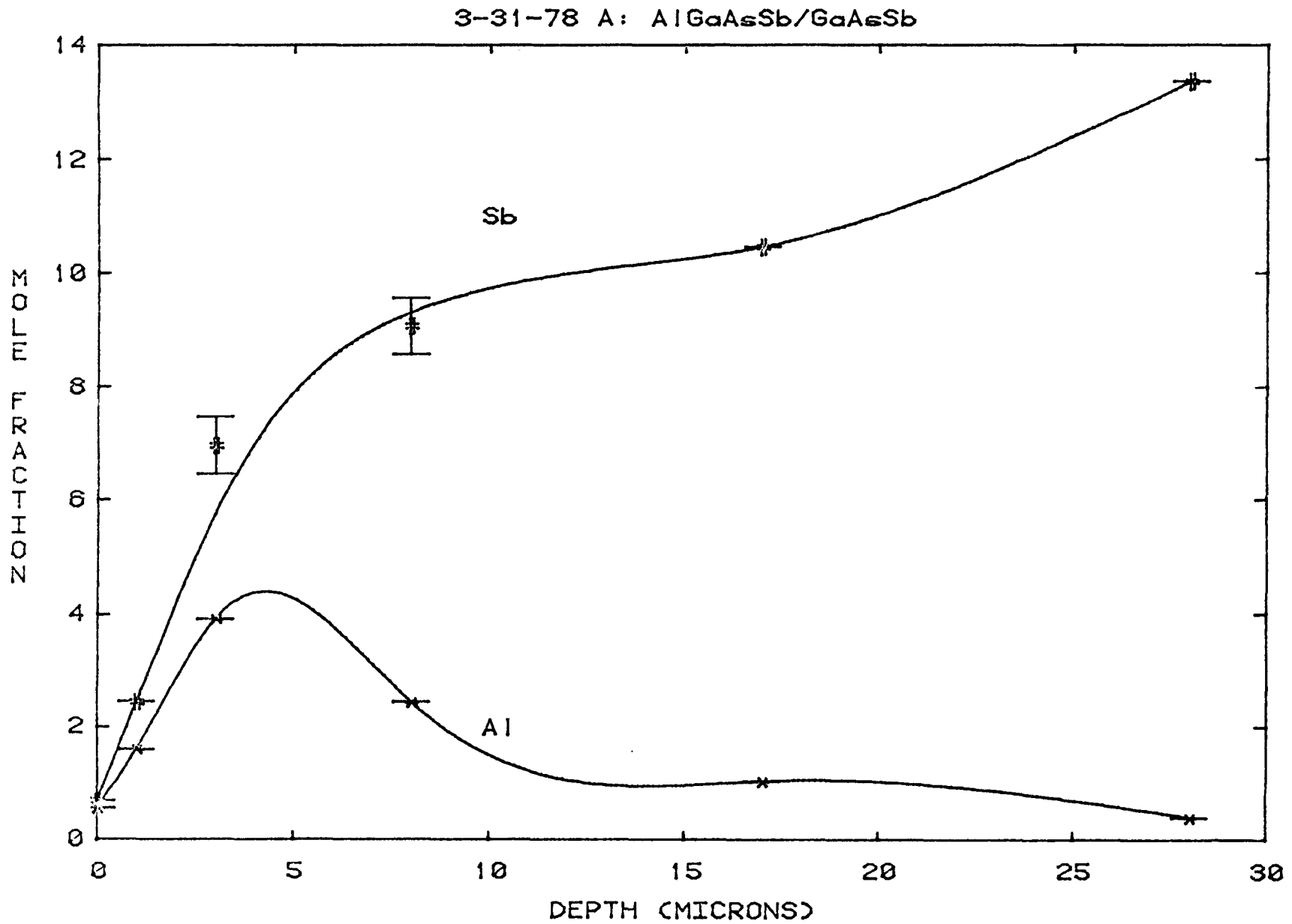

* Al
* Sb

Fig. 5. Concentration profile of Al and Sb across a cleaved section of a continuously graded layer.

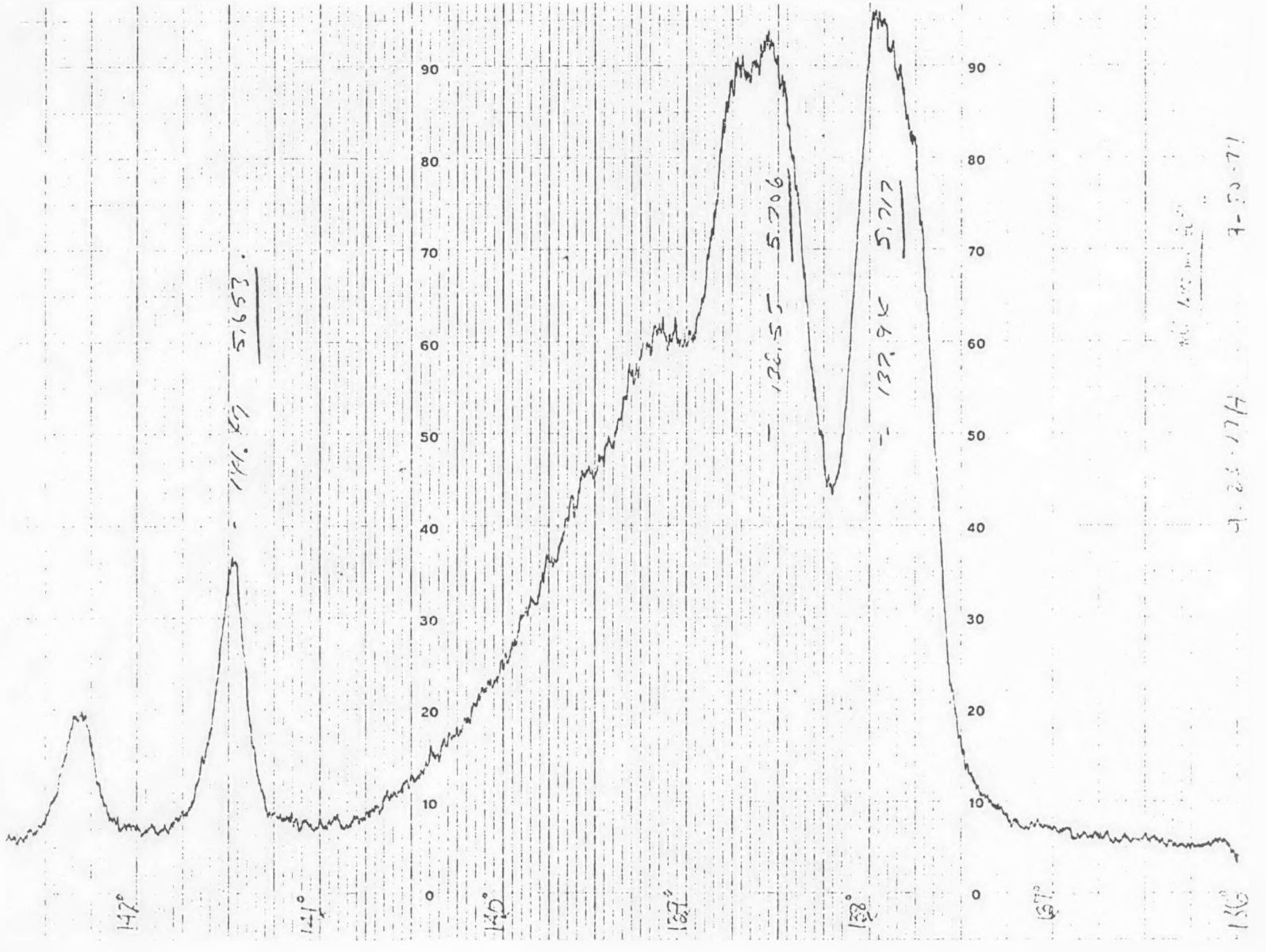

Fig. 6. Diffractometer scan of a continuously graded AlGaAsSb layer with a GaAsSb of a constant composition on top. (444) reflection.

the solution was removed from a portion of the substrate to reveal the surface at that particular temperature. Following growth the wafer then had five shingle-like strips across the surface. The composition of each shingle or strip was determined by electron microprobe analysis, while the thickness of each layer was found by microscopic examination of a cleaved section. Figs. 7 and 8 summarize these results. Also shown are the Sb compositions vs temperature expected for GaAsSb only.

With the inclusion of the GaAsSb data the function of Al becomes more clearly defined. Beginning at 830°C, one sees that a Ga-As-Sb solution without Al is in equilibrium with a solid containing 8 mole% Sb. If this were placed in contact with a GaAs substrates, mismatch would be accommodated over a very short distance (probably < 1 micron) and would produce poor quality layers. However, with Al present in the solution the grading to the equilibrium composition occurs over 6-8 microns, until T ~ 816°C. After the grading portion is complete, Sb incorporation appears to proceed at the rate dictated by the equilibrium phase diagram for a solution containing a ratio of Sb/Ga = 2.5. During this temperature interval, Al incorporation in the column-III sublattice decreases, presumably due to depletion in the solution, while Ga increases. Because the concentration of Sb or As in the solid determines in large part the lattice constant of the quaternary (a_o), rapid variation in the value of a_o occurs first, followed by a slowly increasing value for the remainder of the growth. Thus the growth of AlGaAsSb can be divided into a grading interval followed by an equilibrium deposition region.

The exact thickness of the grading region and position of the Al maximum cannot be accurately determined by electron microprobe analysis owing to the ~ 1 micron^3 sampling volume. By angle lapping the sample and using Auger analysis with a beam size of 0.2 micron and a penetration depth of ~ 100 Å an accurate

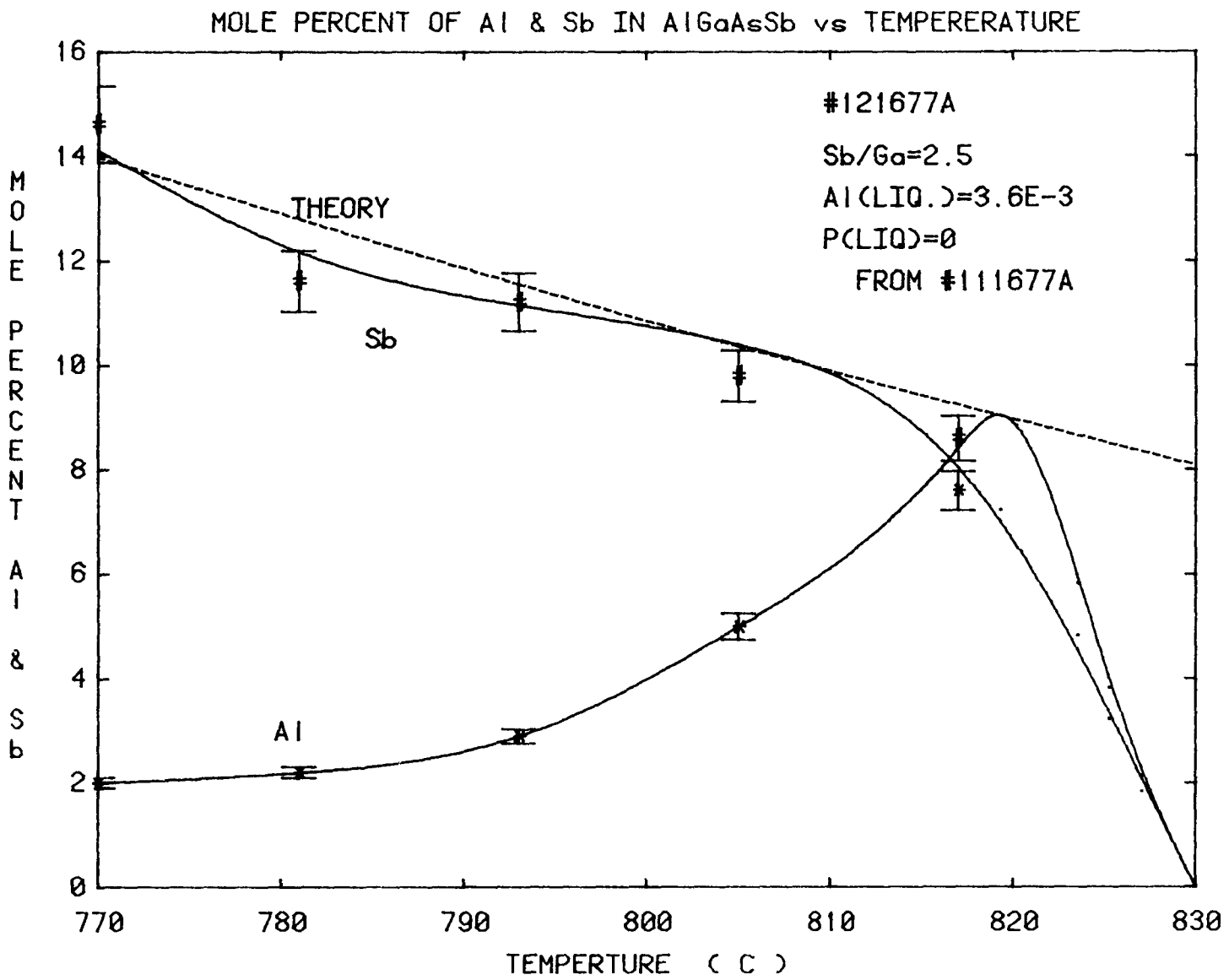

Fig. 7. Mole percent of Al and Sb in AlGaAsSb vs temperature for a continuously graded layer.

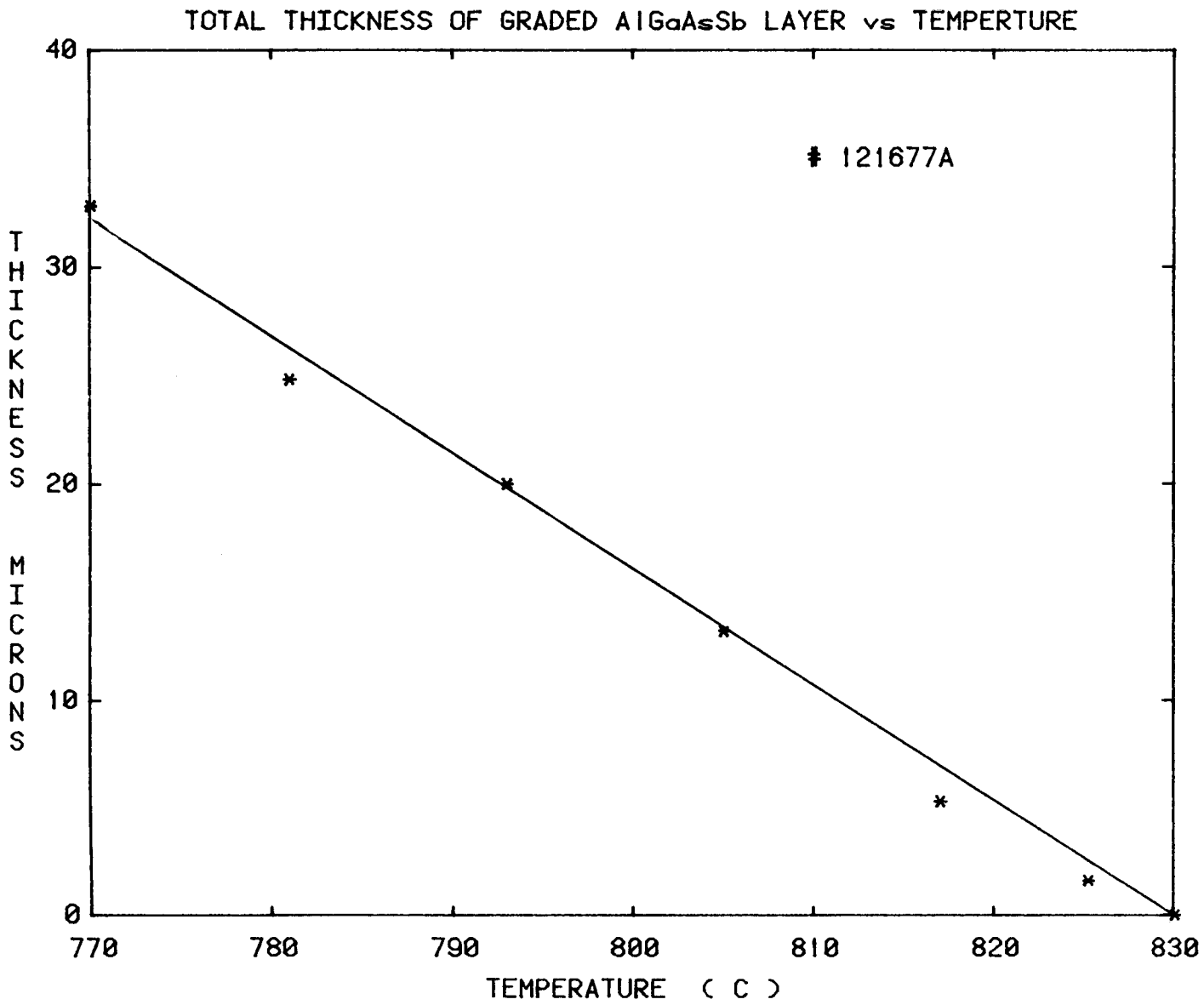

Fig. 8. Layer thickness vs temperature for the graded AlGaAsSb layer in Fig. 7.

determination should be possible. However, this analysis is not yet completed.

We also explored whether the first micron or so of deposition is mismatched, by growing on the (111)A and (111)B surfaces over a temperature interval of only 5°C; thickness on the (111)A and (111)B faces were 1.6 and 0.8 microns, respectively. A very fine cross-hatched pattern indicative of close lattice matching (usually indicative also of compressive stress in the layer) is observed and is shown in Fig. 9.

If further layers are grown by ramp cooling for 5 or 10°C followed by 10 min holding times, striations are observed on a cleaved section for each holding period and some surface morphology improvement is seen. Holding for 30 min between a 5°C temperature decrease often produces a very smooth surface with a cross-hatched pattern after a total cooling of 60°C. The improvement is believed caused by the reduction in concentration gradients developed during continuous cooling. Such gradients lead to compositions that are no longer in equilibrium with the surface and higher defect densities result from the ensuing high rate of change of lattice constant.

Grading now appears to be dictated by two regions which may be varied somewhat independently. The point at which the grading composition intersects the equilibrium composition roughly determines the temperature interval or layer thickness over which most of the grading occurs. By varying the Sb/Ga ratio and temperatures, the equilibrium line can be shifted in composition. Changing the Al in the solution should alter the grading in the transient region. When P is added to form a quinary solution the grading rate increases and there is some evidence that the minimum Al concentration in the solid also increases.

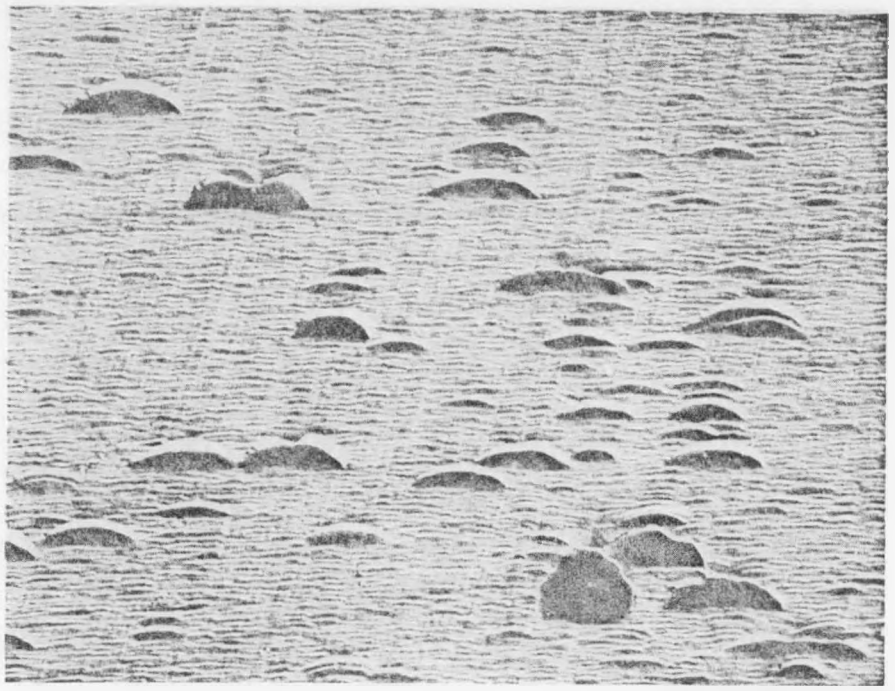

(111)A

(111)B

Fig. 9. Surface morphology of AlGaAsSb layers on GaAs(111)A and (111)B after 5° cooling.

110X

For step cooling over the same temperature interval, solutions designed to produce mole% of 4, 8, 12, and 16 in the solid have been used. Electron microprobe analysis and optical observation of a cleaved section produced the results seen in Figs. 10 and 11; we include the theoretical expectation from the phase diagram. As noted in Sec. 4.2 on orientation effects, grading rate is smaller than the continuous case because layer thickness is greater. Layer thickness no longer varies linearly with temperature as in continuous grading but appears superlinear.

Comparisons to LPE growth models suggest that GaAsSb follows a $t^{3/2}$ law indicative of diffusion-limited growth; a similar time dependence has been reported earlier for single layers of GaAsSb.[6] However, orientation effects suggest that the situation is intermediate between a diffusion and kinetic-limited case. Addition of Al to the solution appears to shift the rate determining step towards one in which the interfacial kinetics are no longer rapid compared to diffusion. Now the layer thickness appears to vary linearly with temperature or time (Fig. 8). This type of dependence will occur from a thin diffusion-limited[7] solution cooled at a constant rate, or from an infinite solution that is limited by interface kinetics.[8] A linear growth rate coupled with an orientation dependence of thickness suggests that AlGaAsSb is rate-controlled by some form of surface kinetics. In part, this is caused by the reduced As solubility.

4.2 Orientation Effects

Influence of substrate orientation on the final layer morphology has been investigated for both continuously graded and step graded layers using GaAs substrates with (111)A and (111)B and (100) surfaces. In one case, using (111) substrates, growth occurred simultaneously from the same solution on both the A and B surfaces by using half a substrate for each orientation. Growth of AlGaAsSb occurred over 60°C, beginning at 830°C, followed by deposition of GaAsSb for 10°C, at a cooling

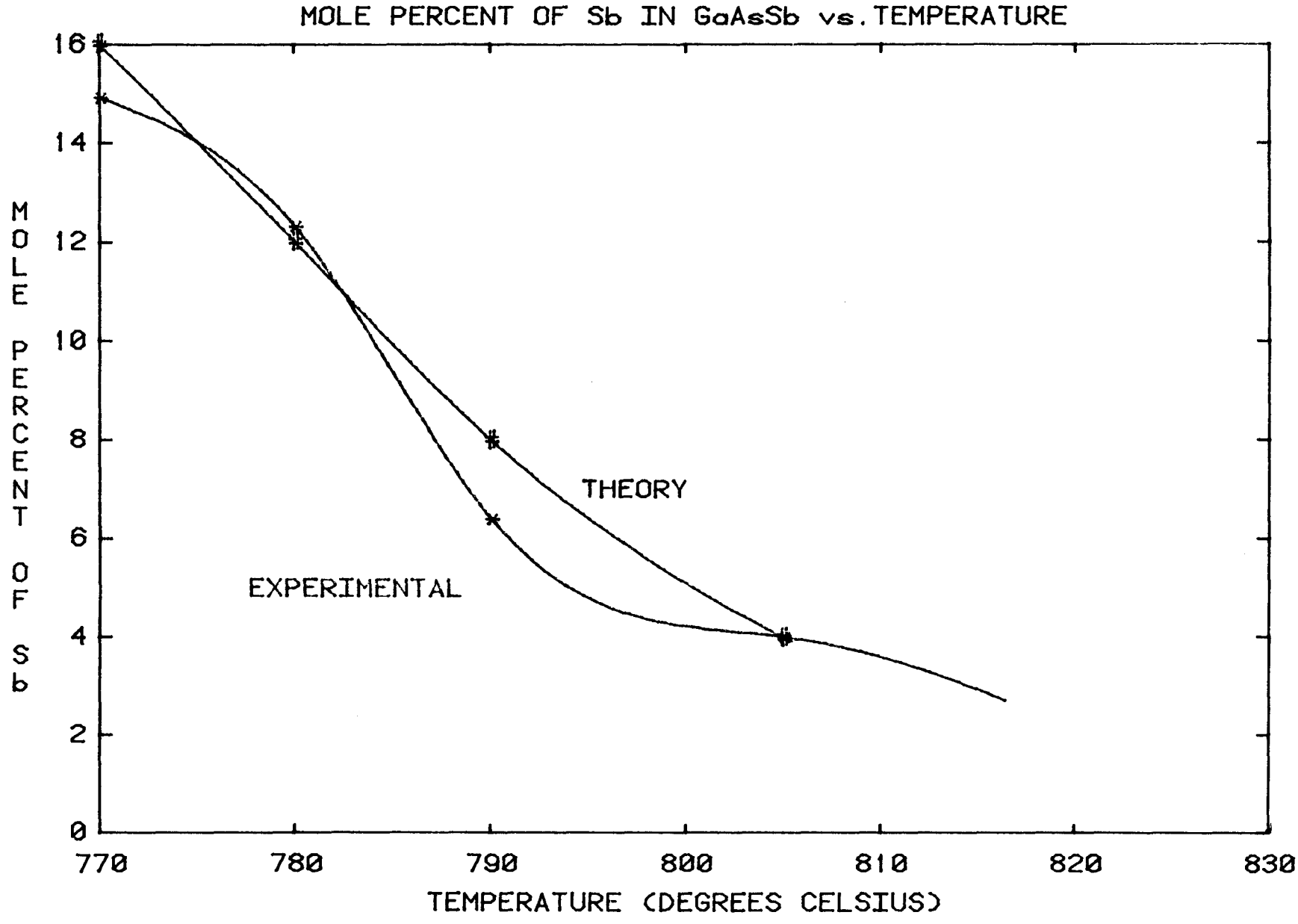

* = EXPERIMENTAL
\# = THEORY

Fig. 10. Mole percent of Sb in GaAsSb vs temperature for step graded layers.

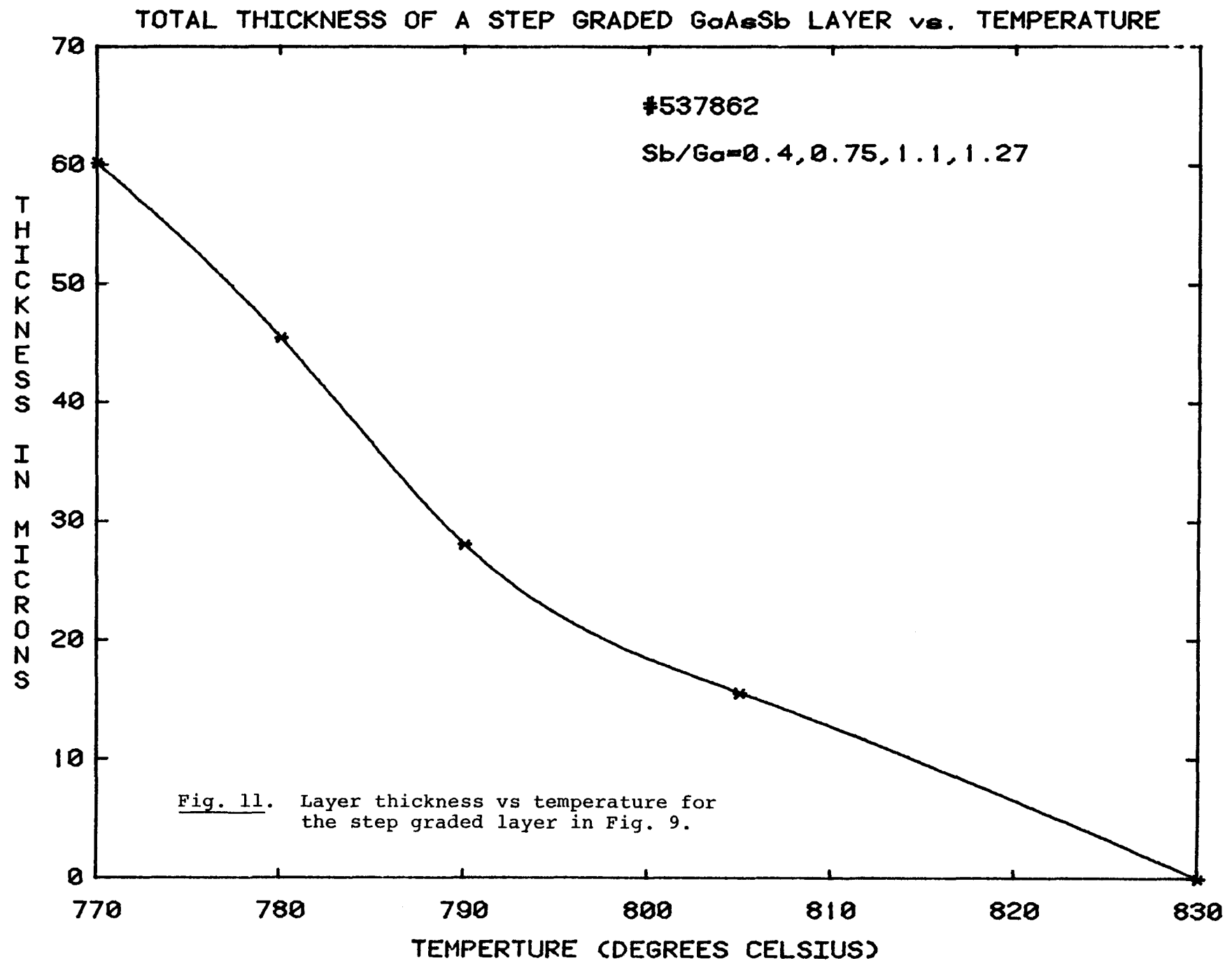

Fig. 11. Layer thickness vs temperature for the step graded layer in Fig. 9.

rate of 0.5°C/min. Thicknesses increased in the order (100) > (111)A > (111)B and are listed along with the average grading rates of Sb in the following table:

	Continuously Cooled		
Orientation	T(AlGaAsSb) (μm)	T(GaAsSb) (μm)	Sb/Δx (a/o/μm)
(100)	22	10	---
(111)A	17	8.3	0.40
(111)B	8.9	2.5	0.88

Solution composition is at a ratio of Sb/Ga = 2.5.

Surface morphologies are shown in Fig. 12 for the three faces. Substrates with a (111)A orientation produce the smoothest surface, while hillocks mark the (111)B orientation and mesa-like mounds covered the (100). Closer examination reveals stacking faults (slashed lines) on the (111)B due presumably to the high grading which requires higher mismatch accommodation per layer thickness.

In the step-graded case solutions that divided the compositional change from GaAs to $GaAs_{.84}Sb_{.16}$ into four equal steps have been used. Deposition occurred over the same temperature interval as in the continuously-graded case. For the (111)A and (111)B case the same disparity in growth rate is observed. However, because Al is absent in all the layers As solubility is much greater and hence so is layer thickness. A similar table as above for layer thickness vs orientation is given below.

	Sb/Ga Ratio				
Orientation	0.4	0.75	1.1	1.27	Sb/Δx (a/o/μm)
(111)A	18.9	15.0	20.4	19.4	0.24
(111)B	13.2	7.5	4.3	---	0.41

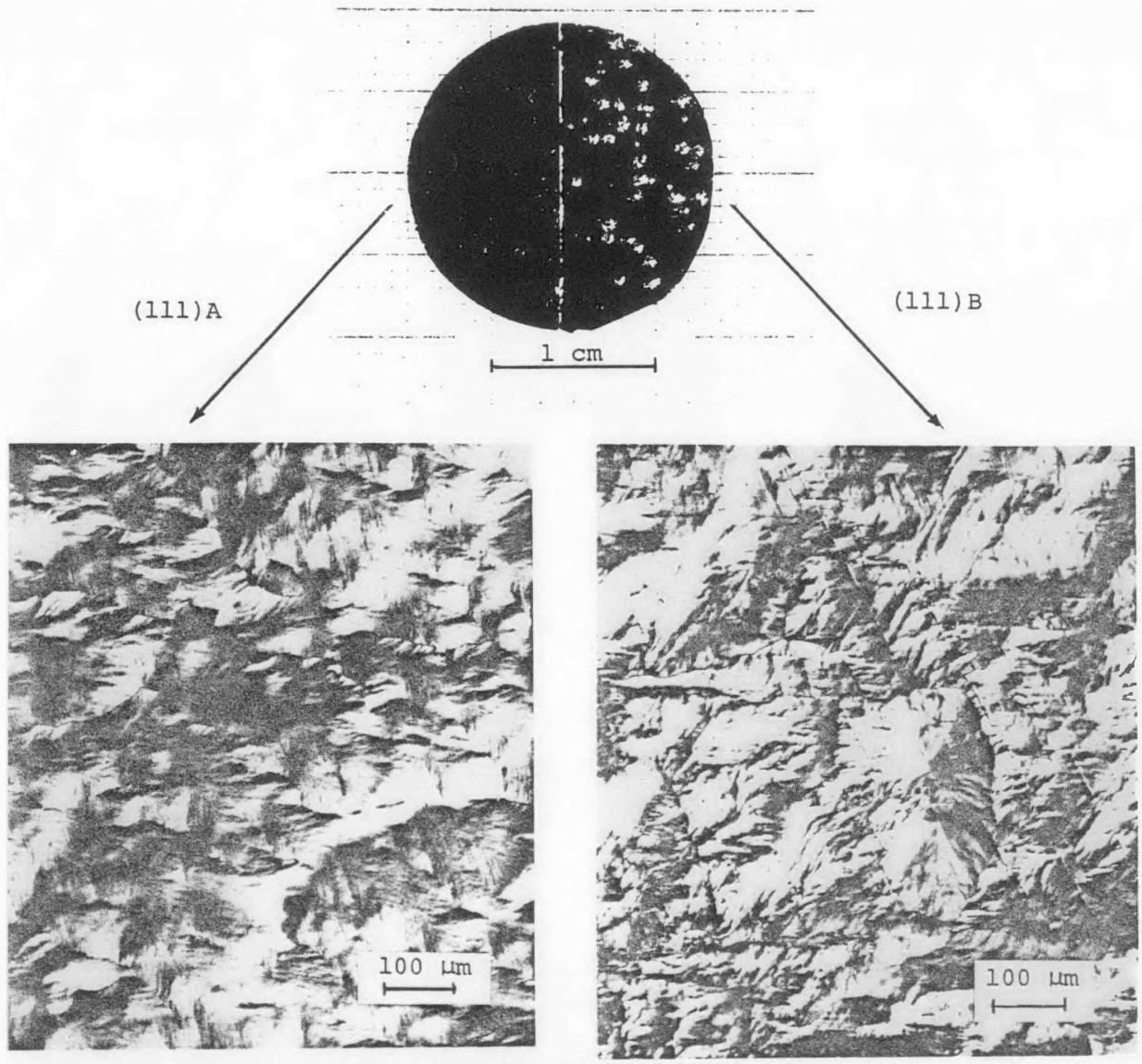

Fig. 12.

Surface morphology of GaAsSb/AlGaAsSb (continuously graded) layers grown on different GaAs substrates.

The slower grading rate appears to be on substrates with a (111)A orientation, providing a grading rate around one half that observed on the (111)B face.

4.3 Surface Morphology as a Function of Sb/Ga Ratio

Surface morphology of layers grown by continuous grading on the (111)A surface of GaAs has been seen to change with Sb/Ga ratio. Surface appearance on either side of the pseudo-binary at Sb/Ga = 1.6 and 2.5 are somewhat different. The Ga rich side is more mound-like and the Sb and As rich side is more feather-like in structure. Increasing the ratio of Sb/Ga to 4 improves morphology and often causes wave-like growth that is often observed on LPE homoepitaxial surfaces. However, at the stoichiometric composition, Sb/Ga $\simeq$ 1.78, a deterioration is seen; sometimes inclusions and at other times many hillocks are observed. Figure 13 summarizes the patterns observed under the various conditions. All of these phenomena are believed caused by variations of X_{As}^{ℓ} that is minimum in the stoichiometric region. This variation is likely to cause changes in the surface kinetics and element diffusivities.

Growth on different faces at the stoichiometric compositions yield nearly complete solution wipe-off from a (111)A surface, total solution adherence on a (100) orientation and no growth on a (111)B substrate. In order to produce growth on (111)B surfaces an increase in cooling rate from 0.5°C/min to 1°C/min is necessary. Presumably, the interfacial kinetic limitations on (111)B surfaces are more severe than on other surfaces examined.

Comparison by x-ray topograph of a GaAsSb/AlGaAsSb(graded)/GaAs(111)A structure grown from a solution with Sb/Ga = 2.5 and 4.0 are seen in Fig. 14. For the Sb/Ga = 2.5 case the topograph is characterized by a cellular structure indicative of small-angle grain boundaries, while from the solution with a higher

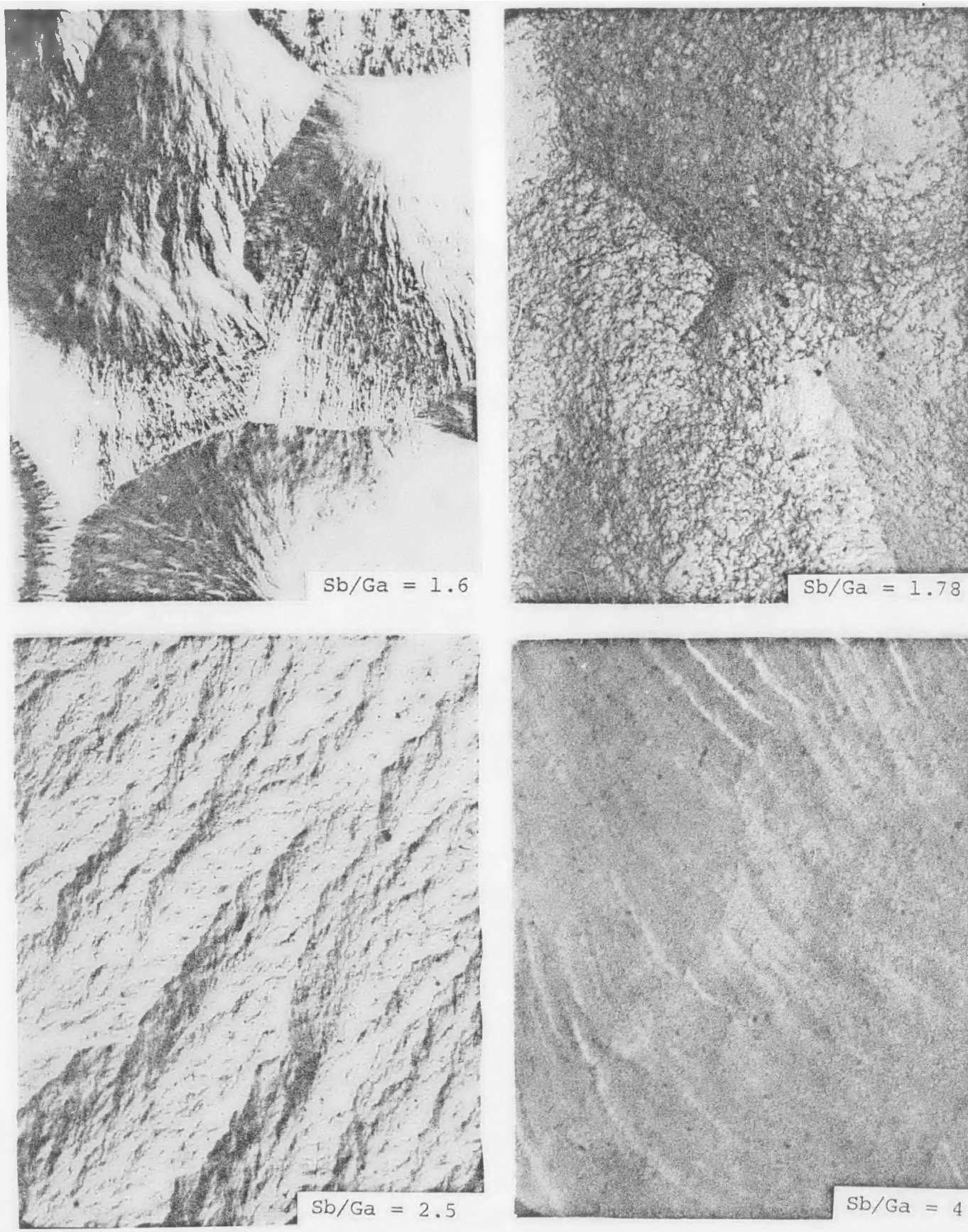

Fig. 13. Surface morphology of continuously graded AlGaAsSb/GaAs (111)A grown from solutions with different Sb concentrations. 110X

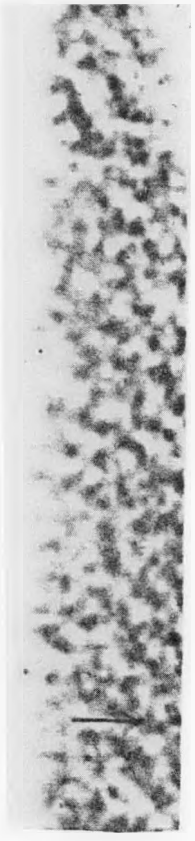

Sb/Ga = 2.5

GaAsSb/AlGaAsSb

(3.6μm) (8.7μm)

(a)

Sb/Ga = 4.0

GaAsSb/AlGaAsSb

(2.9μm) (20.7μm)

(b)

Fig. 14. X-ray topographs of GaAsSb/AlGaAsSb (graded)/GaAs(111)A grown from solutions with Sb/Ga ratios = 2.5 and 4.

As solubility (Sb/Ga = 4.0) a cross-hatch pattern is observed. Possibly this is caused by a finer nucleation so fewer dislocation networks occur when larger growth islands agglomerate.

5. ETCH PIT STUDIES

At the beginning of this program, etch pit studies were made to ascertain the general density observed in continuously graded layers. Dislocation densities at the surface of the GaAsSb/AlGaAsSb/GaAs(111)A structure have been measured on nine samples grown from a solution with Sb/Ga = 2.5. These densities vary by no more than an order of magnitude from each other and are never less than 10^6 cm^{-3}. A summary of the results are shown in the table below.

Dislocation Density

Sample No.	Dislocation Density x 10^{-6} (cm^{-2})
920A	5 to 14.5
921A	3 to 7.5
922A	6 to 10
923A	4 uniform
929A	21
1019A	8 to 15

From these results it is inferred that dislocations are generated during the growth process since typical substrate dislocation densities are 10^4 cm^{-2} and seldom exceed 10^5 cm^{-2}. Besides dislocation propagation from the substrate, dislocation generation during epitaxial growth can occur when misorientated nuclei coalesce, by plastic deformation of the film, or by condensation of point defects.

Two etches have been used: the normal "A" etch solution ($1HF:5HNO_3:12AgNO_3$(1%)) and an etch developed for AlGaAs ($1H_2O:1H_2O_2:2CH_3COOH:0.5HF$).[9] A 1:1 correspondence between

both etches is seen, although the acetic-acid-based etch is easier to control and produces better formed pits on GaAs, AlGaAsSb, and GaAsSb with (111)A surfaces.

If dislocation distribution were uniform at 10^6 cm^2, then the average distance between dislocations would be 10 microns, a distance not likely to limit minority carrier diffusion length. Unfortunately, this is not true in general and a bunching of dislocation to densities $> 10^7/cm^2$ are observed. An example of the inhomogeneity that can exist is seen in Fig. 15.

To begin an investigation of defects seen in graded layers the influence of substrate dislocation density was examined. Two substrates were grown on simultaneously, one with a density of 1.8×10^4 cm^2 and the other with a density of 9.7×10^4 cm^2. Layer deposition consisted of a graded layer of AlGaAsSb (20 microns) with a GaAsSb (16 microns) deposited on top. Photomicrographs of the surfaces before and after are seen in Fig. 16. Dislocation density after growth is 2×10^7 cm^{-2} and $4\text{-}6 \times 10^7$ cm^{-2} suggesting that a factor of 2 to 3 between the final density may occur when the starting density differs by 5.

These figures suggest that as the dislocation density increases so does the tendency to form the triangular figures seen in Fig. 17. In extreme cases these triangles form thick sides that look like large slip bands. It is not clear yet whether these large bands are precursors to cracks or not, whether they depend on a tensile stress condition in the layer or just on the dislocation density.

In an attempt to understand the origin of these defects a sample was progressively etched back from the surface using $NaOCl:H_2O$ solutions. The results shown in Fig. 17 indicate that formation takes place early in the continuous grading

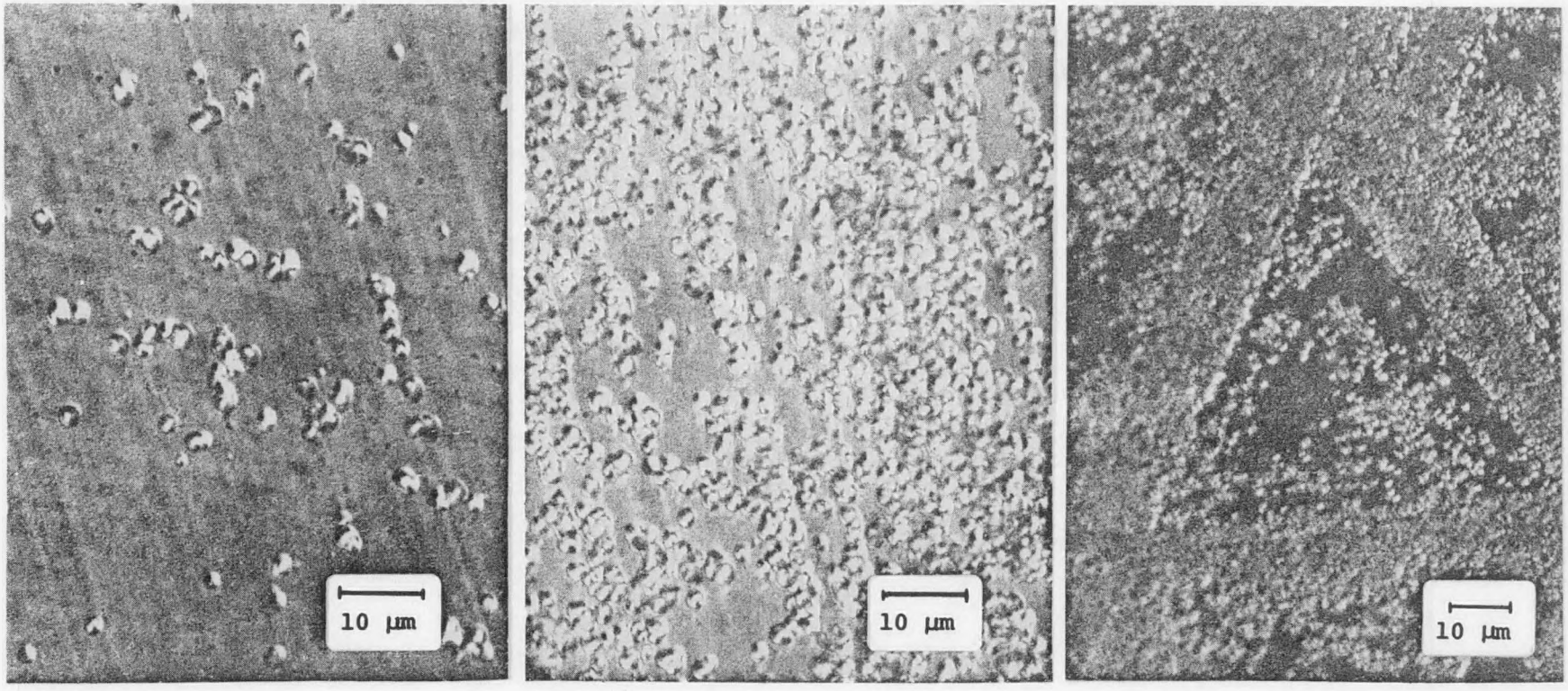

Fig. 15. Types of etch pit distributions observed on GaAsSb/AlGaAsSb/GaAs(111)A. Solution ratio of Sb/Ga = 4.

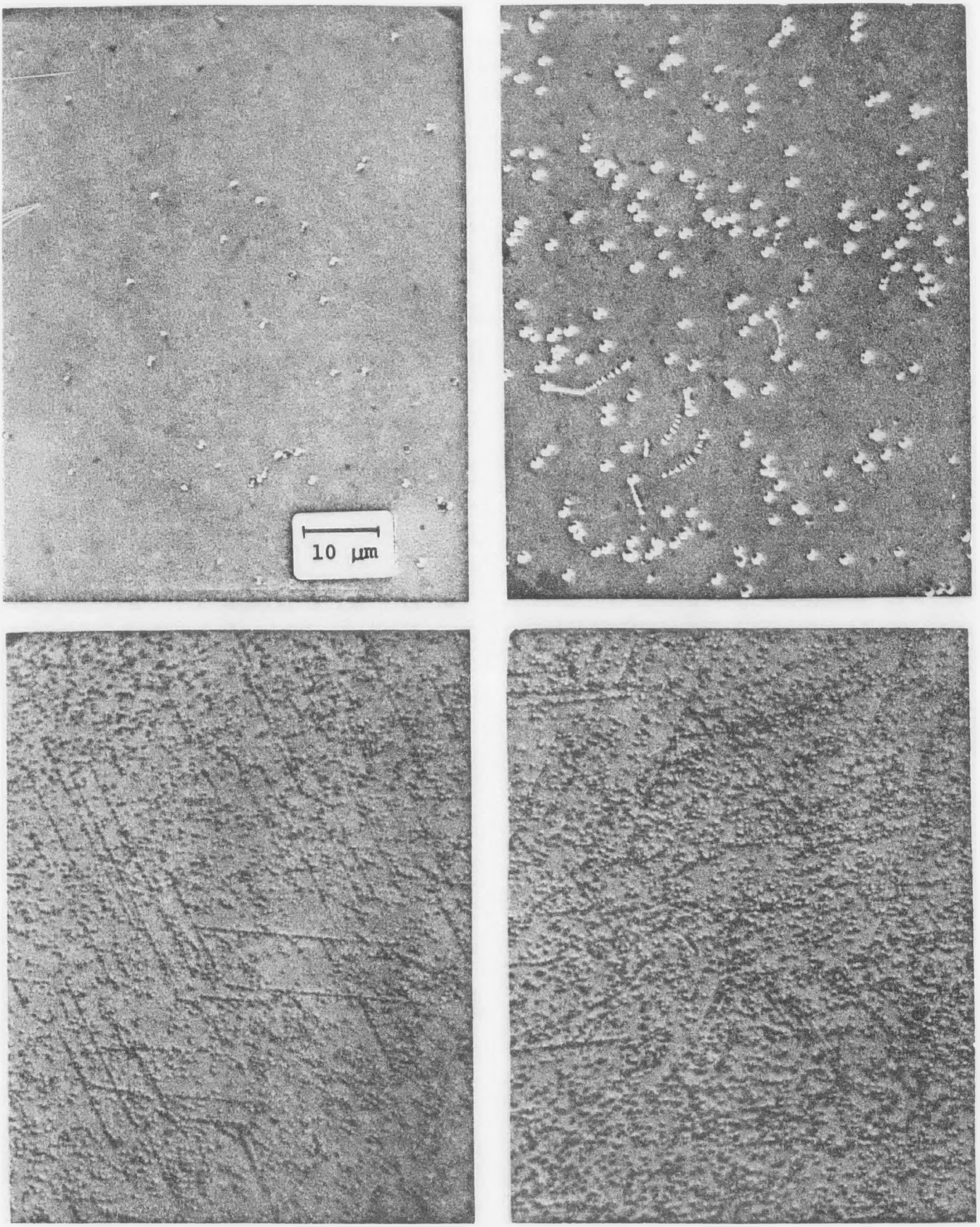

Fig. 16. Dislocation densities observed before and after growth of GaAsSb/AlGaAsSb (graded) layers Sb/Ga = 4. #42878A
Substrate dislocation density: Column I 1.7×10^4 cm^{-2}
Column II 9.7×10^4 cm^{-2}

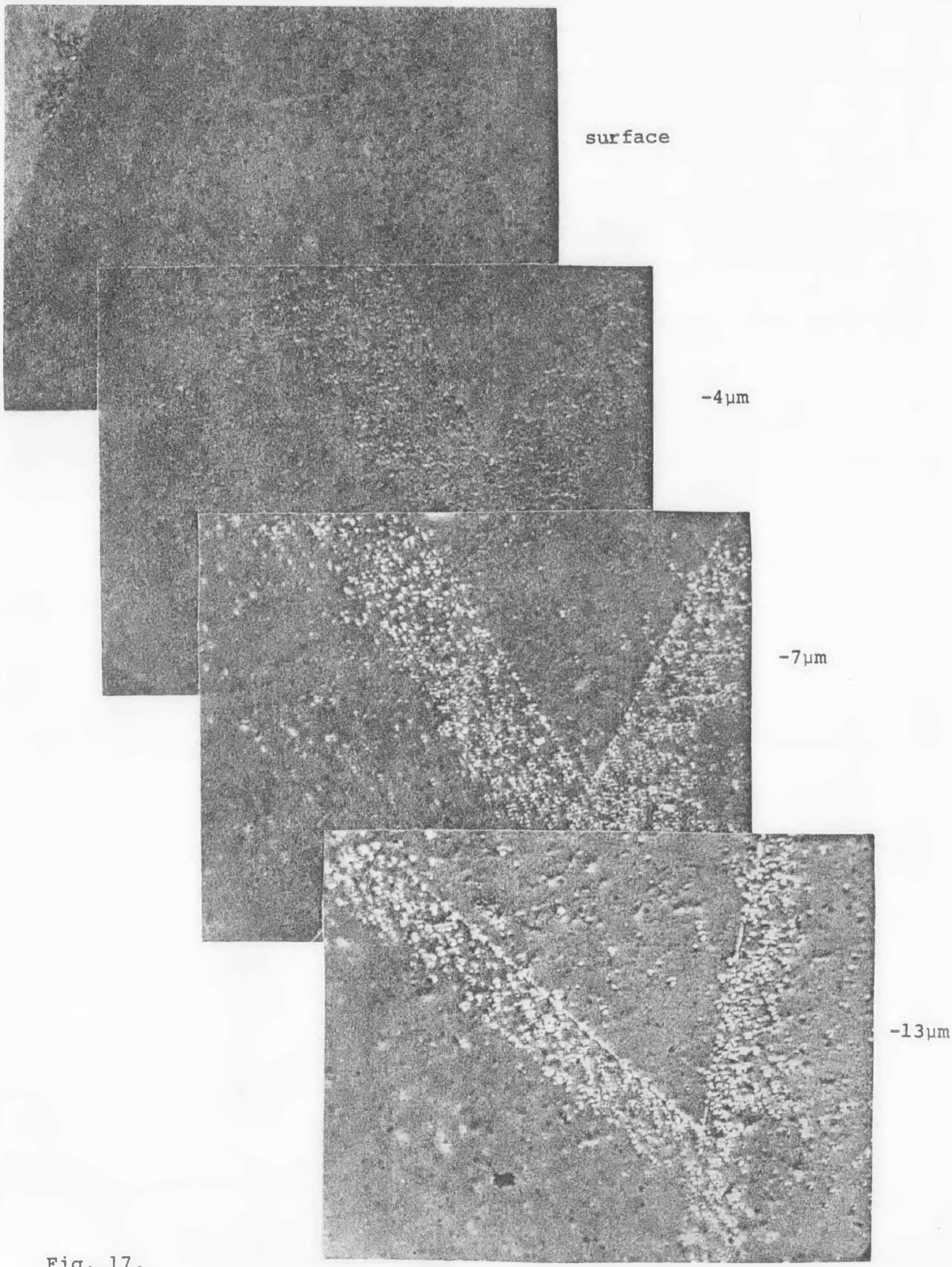

Fig. 17.

portion of growth. Also seen is the impenetrability of the triangles, which suggest a barrier to dislocation motion such as a stacking fault. This is now being examined in greater detail.

6. DISLOCATION BUNCHING

Dislocation morphology at the beginning of growth helps explain the later distribution. A single layer of $GaAs_{.96}Sb_{.04}$ was deposited on a GaAs(111)A substrate at ~ 730°C. Under the conditions used, growth was not complete over the entire wafer and dislocation distributions in the early stages were revealed.

Inspection of the as-grown surface shows minor undulations which when a portion is etched reveals bunches of dislocations (see Fig. 18). Turning now to the partially-grown region, several illuminating features are observed. The three main features are seen in Fig. 19. In the upper left-hand corner is a small island with a dense population of etch pits, in the middle an organized array of pits, and at the lower right-hand corner a large island partially covered with etch pits. The areas not covered by pits are either the substrate or a very thin epitaxial layer that has not lost its coherency. Examination of a cross-section shows very thin wedge-shaped layers sloping away from the large islands. Most of the large islands have very ordered arrays at their edges, while the smaller triangular-shaped islands seldom do.

The ordered array in the center of Fig. 19 is possibly caused by the thin layer being slightly thicker at that point so that the coherency thickness has been exceeded.[10] The necessary mismatch dislocations have glided in from the surface to form half loops. Whether the resultant inclined dislocations cause an enhanced growth rate at this point to form a small island cannot be ascertained. In any event, once these small islands begin to grow in both the lateral and perpendicular directions relative to the surface the inclined dislocations appear to stay near the island's edge. Either new mismatch dislocations glide in from the edge of the island or as the island thickens the inclined dislocations already present move under

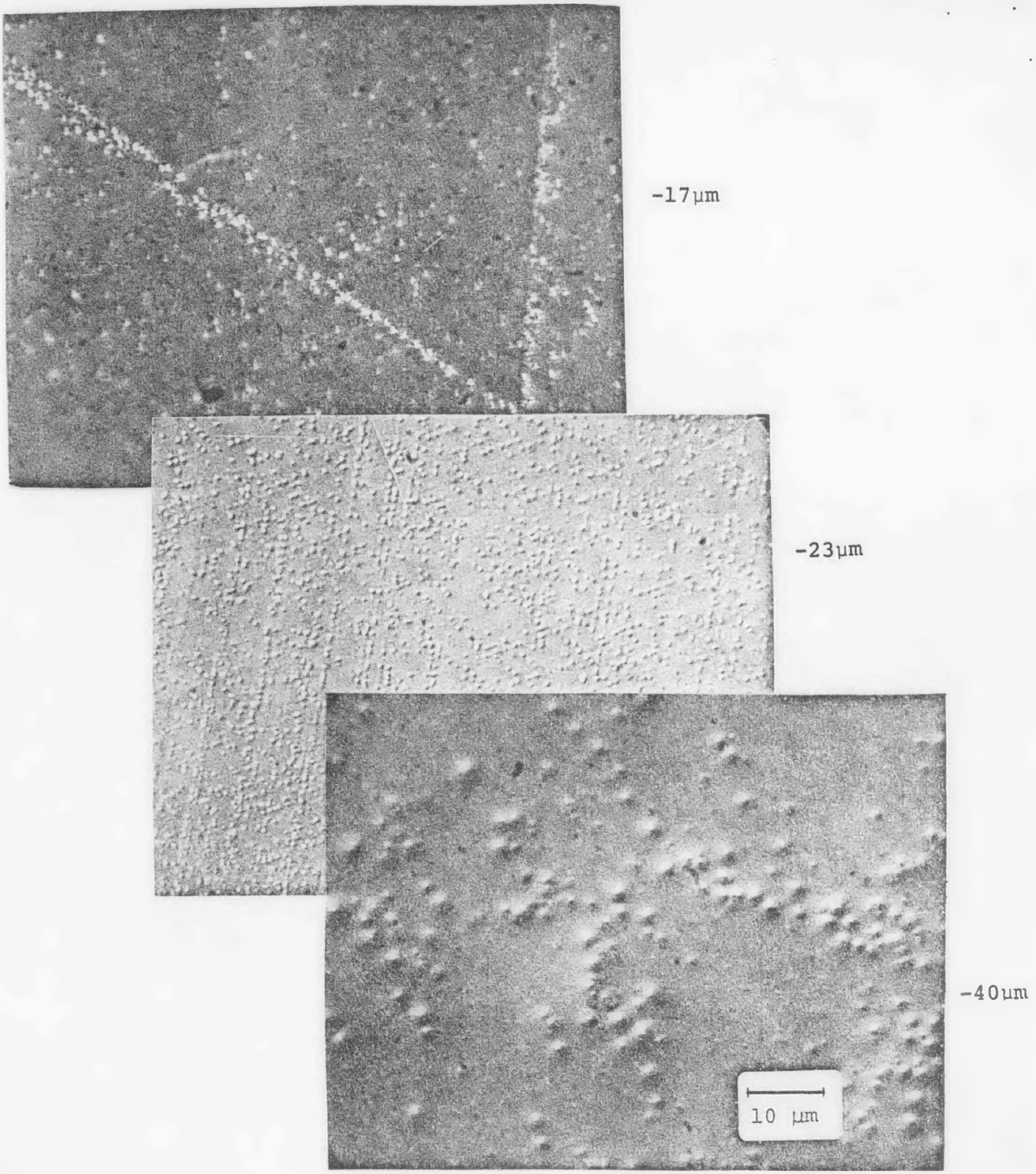

Fig. 17. Dislocation morphology as a function of depth in a GaAsSb/AlGaAsSb(graded)/GaAs(111)A structures. #42078A

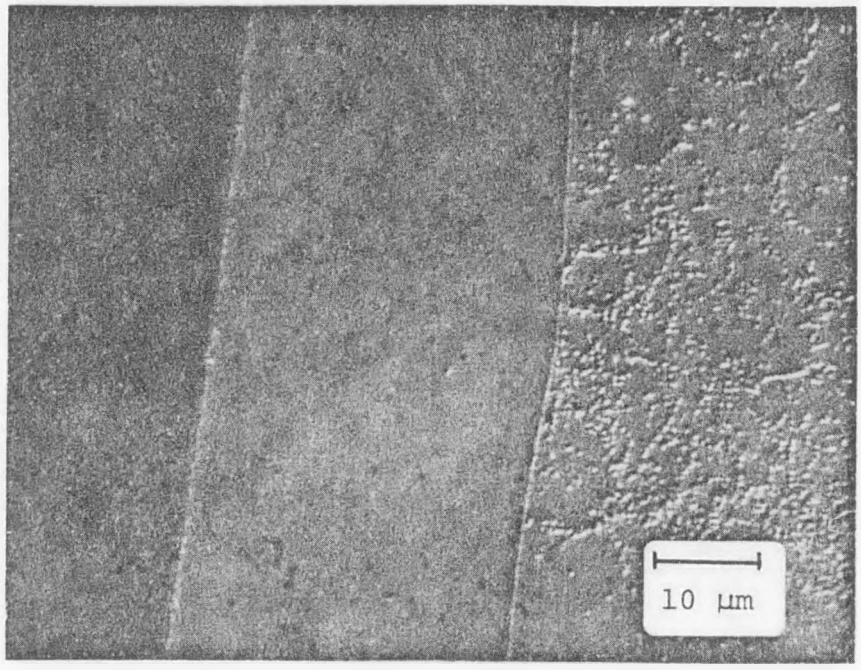

Fig. 18. Surface of a single layer of $GaAs_{.96}Sb_{.04}$ grown on GaAs(111)A showing an etched and unetched region. (#51078M)

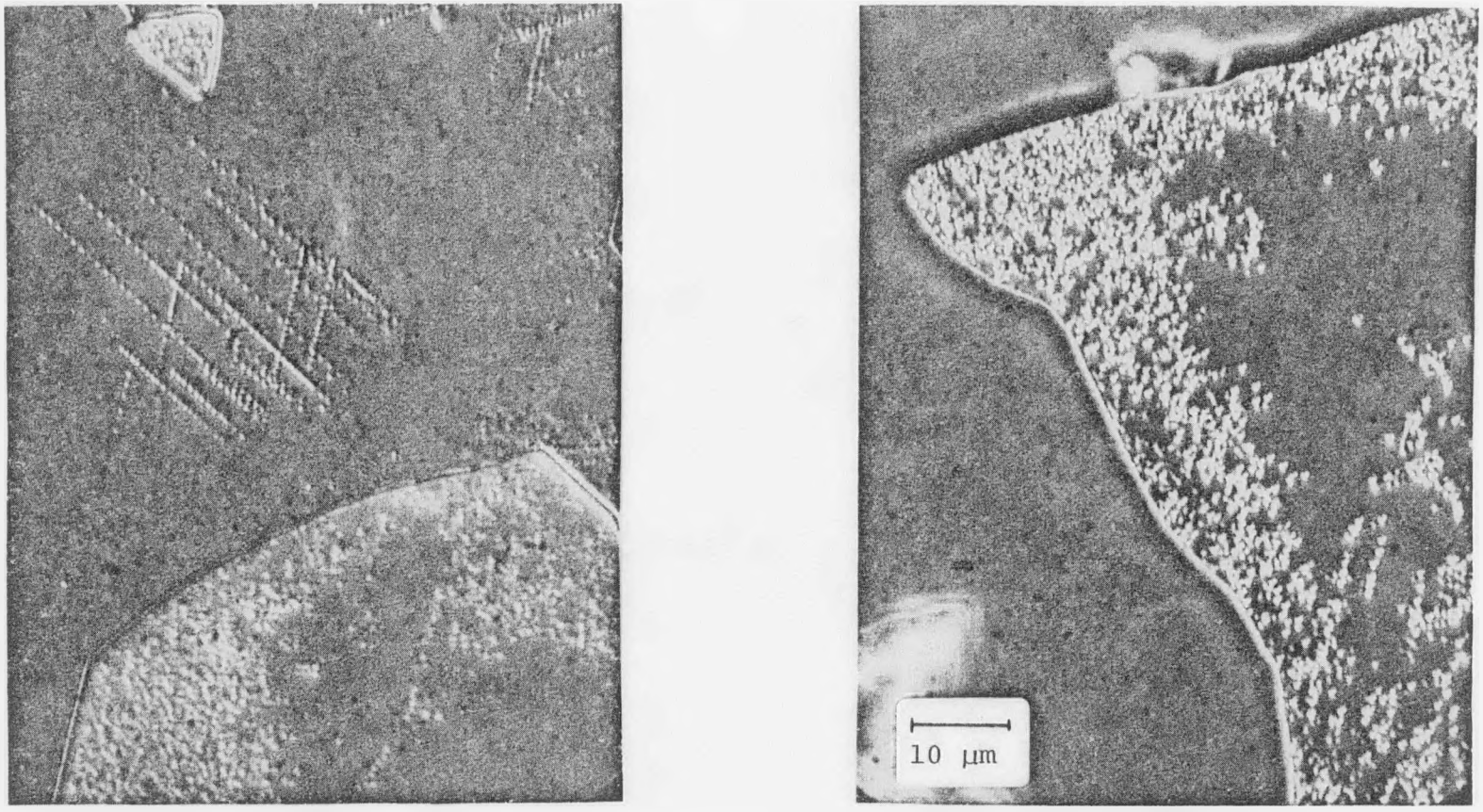

Fig. 19. Etch pits observed in growth islands, and thin layers in a region not completely covered by the GaAsSb layer shown in Fig. 18. (a) Main features showing small and large growth islands and mismatch dislocations. (b) Large islands with peripheral etch pits.

the additional forces caused by growth to form additional lengths of mismatch dislocations. As larger islands meet, dislocations near the edge of each island and those just preceding them are seen to bunch together (Fig. 20).

It would appear that if either layer growth could be maintained throughout grading or that finer nucleation could be achieved, then a more uniform dislocation distribution would result. Although the example examined is a single layer mismatched from the substrate, the general ideas may still apply during a continuously-graded growth. Possibly the more uniform dislocation distribution often, but not always, seen when continuously-graded growth is periodically interrupted is in part due to the limiting of large island size. This would be caused by ensuring that concentration gradients which would lead to few nuclei are not too severe.

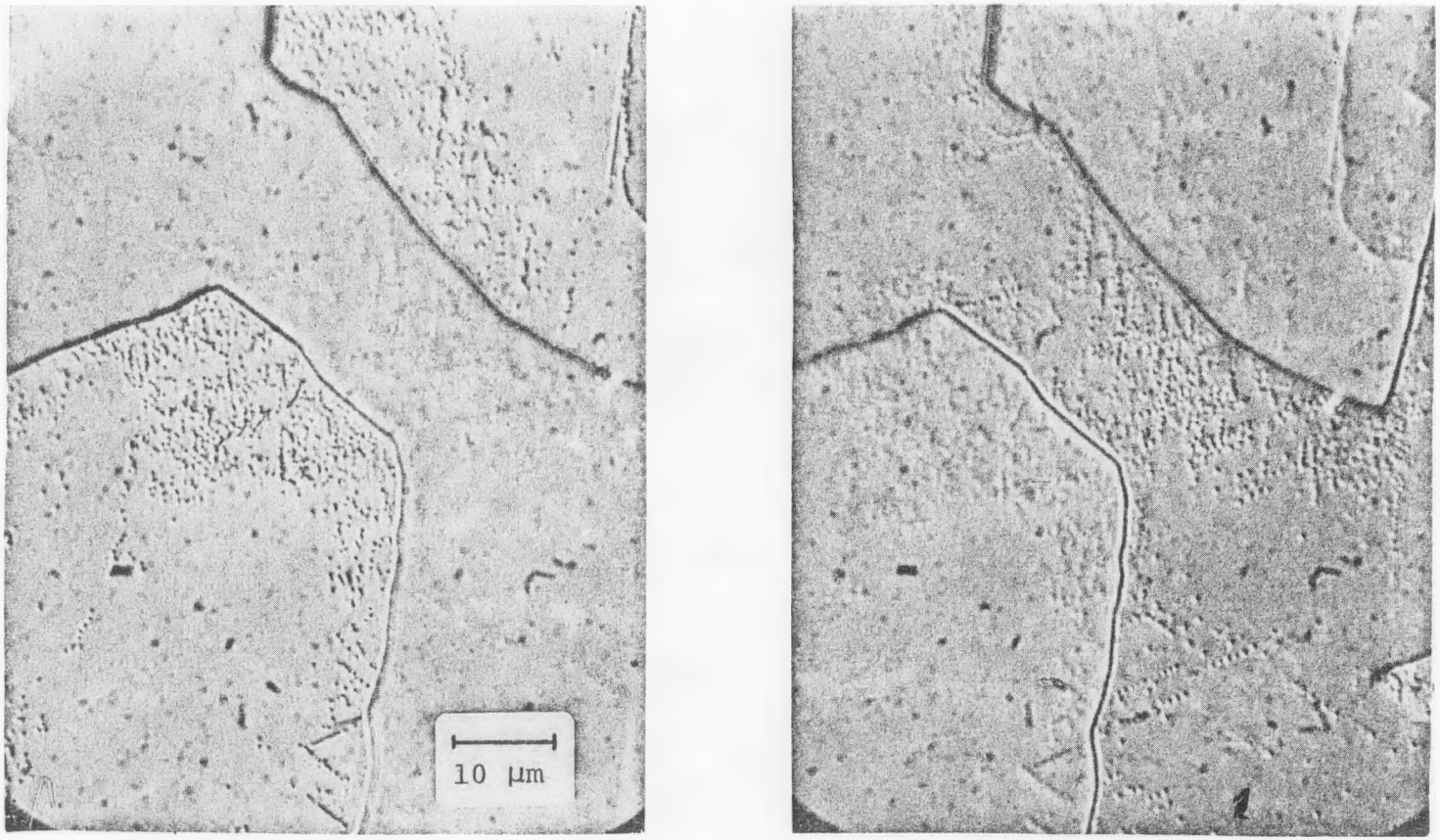

Fig. 20. Large growth islands just before agglomeration.

7. DOPING OF GaAsSb

7.1 Tin Doping

Tin has been chosen as the n-type dopant rather than Te because there are no reported compounds formed between it and any column-III or V elements at the growth temperatures used. In the Te case, GaTe (mp 824°C), Ga_2Te_3 (mp 790°C), and Al_2Te_3 (mp 895°C) are examples of compounds which can form precipitates in AlGaAs at the 10^{18} cm^{-3} concentration level. More important is that Te is known to deteriorate surface morphology and solution removal in AlGaAs.[11]

Samples consisting of a graded AlGaAsSb layer followed by a layer of $GaAs_{.84}Sb_{.16}$ have been grown in the normal manner on Cr-doped GaAs(111)A substrates. Results of these doping studies are tabulated in the following table for a solution containing a weight ratio of Sb/Ga = 2.5 in both the graded and constant composition layers.

Carrier Concentration and Mobility at 300°K and 77°K for a $GaAs_{.84}Sb_{.16}$/Graded AlGaAsSb

	300°K		77°K		
X_{Sn} (at. fraction)	N_D-N_A (cm^{-3})	μ (cm^2/V-sec)	N_D-N_A (cm^{-3})	μ (cm^2/V-sec)	#
$8.4x10^{-3}$	$8.3x10^{16}$	2989	$6.79x10^{16}$	2914	2678A
$4.1x10^{-2}$	$5.2x10^{17}$	2457	$5.1x10^{17}$	2591	1678A
$7.8x10^{-2}$	$9.3x10^{17}$	2383	$9.6x10^{17}$	2418	92977B

Examination of the table shows a near constant carrier concentration and mobility with temperature, similar behavior also has been observed in Sn-doped $Al_{.2}Ga_{.8}As$ at an electron concen-

tration of 4.5×10^{17} cm^{-3}. [12] Behavior of this type in the AlGaAs case is attributed to metallic impurity conduction where the impurity band has merged with the conduction band and the ionization energy has gone to zero. The mobilities observed here are on the average 63% of those observed in GaAs but about 30% higher than $Al_{.2}Ga_{.8}As$ with an electron concentration of 4.5×10^{17} cm^{-3}.

Although carrier concentration and mobility have been measured on a composite layer containing a region of changing composition, these values are still considered a good representation of the doping behavior. For example, doping of AlGaAs with Sn shows that for a given mole fraction of Sn in solution the electron concentration is nearly constant for an AlAs fraction < 20%. From this we infer that Al incorporation in the graded layer probably does not influence Sn incorporation since Al in AlGaAsSb never exceeds 18 mole%.

The segregation coefficient for Sn computed from these data is 2.6×10^{-4}. The value observed for deposition of Sn-doped GaAs with a (111)A orientation is 0.7×10^{-4}. Initially one might expect the electron concentration to decrease for a given amount of Sn in solution as Sb is added because more Sn would be incorporated on the column-V site and act as an acceptor; this would occur because the Sb covalent radius is larger than that of As. However, in this case deposition occurs in the column-V rich region of the phase field, so the column-V vacancy density is expected to decrease and in turn cause more Sn to be incorporated on Al or Ga sites.

Some evidence to support this is obtained from previous work on GaAsSb grown from the Ga rich side of the pseudobinary, but on GaAs(100) Cr-doped substrates. Growth temperatures were 760-740°C with one intermediate step-graded layer. These results and the data above have been included in Fig. 21.

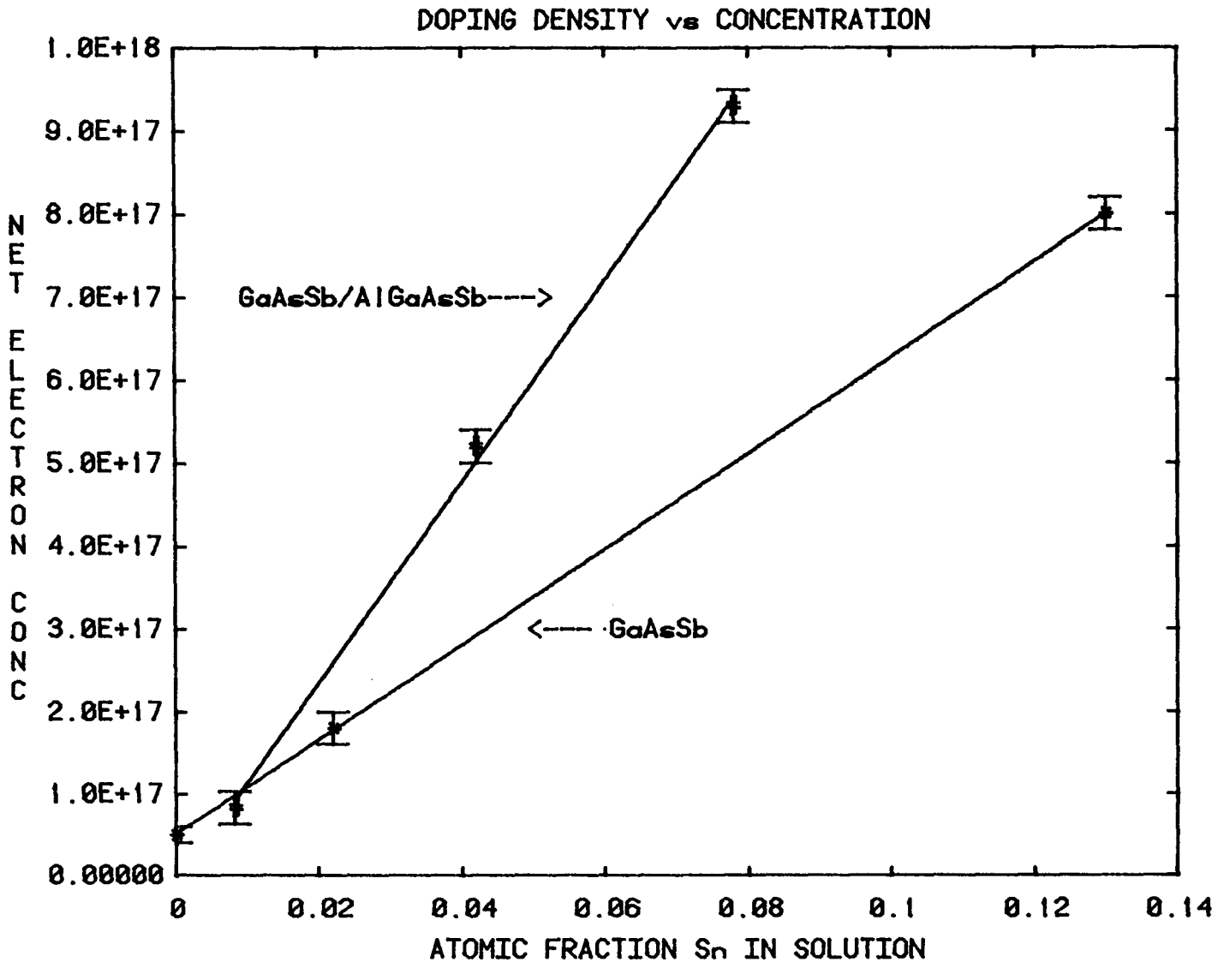

Fig. 21. Doping density vs Sn concentration in solution for growth from the Ga rich and Sb rich sides of the pseudobinary.

Although a (100) face was used, comparison is likely to be valid since Kang and Greene[13] found the segregation coefficient of GaAs at 850°C to be the same for (111)A and (100) orientations ($K \sim 0.7 \times 10^{-4}$).

7.2 Magnesium and Zn Doping

An analysis to determine carrier concentration vs liquid content of Mg and Zn has as yet not been carried out. Preliminary results from p-n junction formation show a behavior similar to that seen in GaAs. Both have been used to form diffused junctions but neither has demonstrated a marked superiority over the other. Characterization of their behavior is planned later in the program.

8. SOLAR CELL PROPERTIES

8.1 Anticipated Performance of the AlGaAsSb/GaAsSb Solar Cell

The first step in fabricating the monolithic solar cell based on AlGaAsSb is to complete the lower junction cell. This consists of an AlGaAsSb window lattice-matched to GaAsSb with a bandgap of 1.15 eV. Bandgap of the window layer must be $\geq$ 1.65 eV.

Modelling of this arrangement for an AlGaAsSb window layer with 60% Al that produces an indirect bandgap alloy and for GaAsSb with a 1.2-eV bandgap has been completed. A bandgap of 1.2 eV , rather than 1.15 eV, has been used because the range of interest lies between 1.15 to 1.25 eV owing to materials considerations. A 0.4-micron deep junction, negligible surface recombination velocity at the hetero-interface, and a contact grid optimized for 1000 suns illumination are assumed. The following table summarizes the results.

Projected Performance at 1 Sun AM2 for an AlGaAsSb/GaAsSb Solar Cell

L_p (μm)	L_n (μm)	V_{oc} (V)	I_{sc} (mA)	F.F.	η (%)	Approx. Maximum QE
5	3	0.71	11.6	0.825	15.4	98*
5	3	0.70	8.6	0.821	11.1	65
1	1	0.70	7.5	0.82	9.7	65
0.5	0.5	0.69	6.2	0.82	7.9	54
0.3	0.3	0.68	4.6	0.81	5.8	40
0.1	0.1	0.649	1.5	0.79	1.7	11

*AR coating included.

The first row shows the behavior expected from a near optimum cell including a single layer Si_3N_4 antireflection coating. Integrated reflectivity is ~ 0.14 but increases to 0.48 if the

same cell is tested without such a coating. As can seen, a single cell of this type with a 2.2-eV window cut-off should yield an efficiency of 15.4% and 11.1% with and without an AR coating at 1 sun at AM2. These efficiencies will be reduced by 0.64 if a 1.65-eV window is used at 1 sun. If 1000 suns illumination and a 1.65-eV window are used, the efficiencies will be 82% of those in the table because the benefits of using a concentrator contact grid are finally realized.

8.2 Performance of GaAsSb p-n Junction and AlGaAsSb/GaAsSb Solar Cells

Examination of I-V curves and quantum yield curves is a rapid means of electrically assessing material quality. Often p-n junctions in GaAsSb are used because any mismatch-associated problems occurring at the AlGaAsSb/GaAsSb interface are avoided. Also, contacting directly to GaAsSb is much easier than to AlGaAsSb.

The ability to produce inclusion-free GaAsSb at 1.15 eV over an area > 0.5 cm^2 is vital to the success of a stacked cell arrangement. Growth conditions must be chosen to maximize the As concentration so that large growth islands are kept to a minimum. After growth, observation of the surface may not reveal any inclusions that have been grown over during the course of layer formation. An example of this and the surface morphological feature associated with a buried inclusion is seen in Fig. 22. Seen in the optical photomicrograph is a seam-like defect which a transmission infrared microscope reveals to be an inclusion.

Improved surface morphology for growth from a solution with Sb/Ga = 4 has been noted earlier. A GaAsSb p-n junction with an area of 0.68 cm^2 was fabricated from this solution and its I-V curve is shown in Fig. 23. Low leakage current indicative of the lack of inclusions is noted. A quantum yield curve of this junction suggests diffusion lengths of ≤ 0.5 micron in

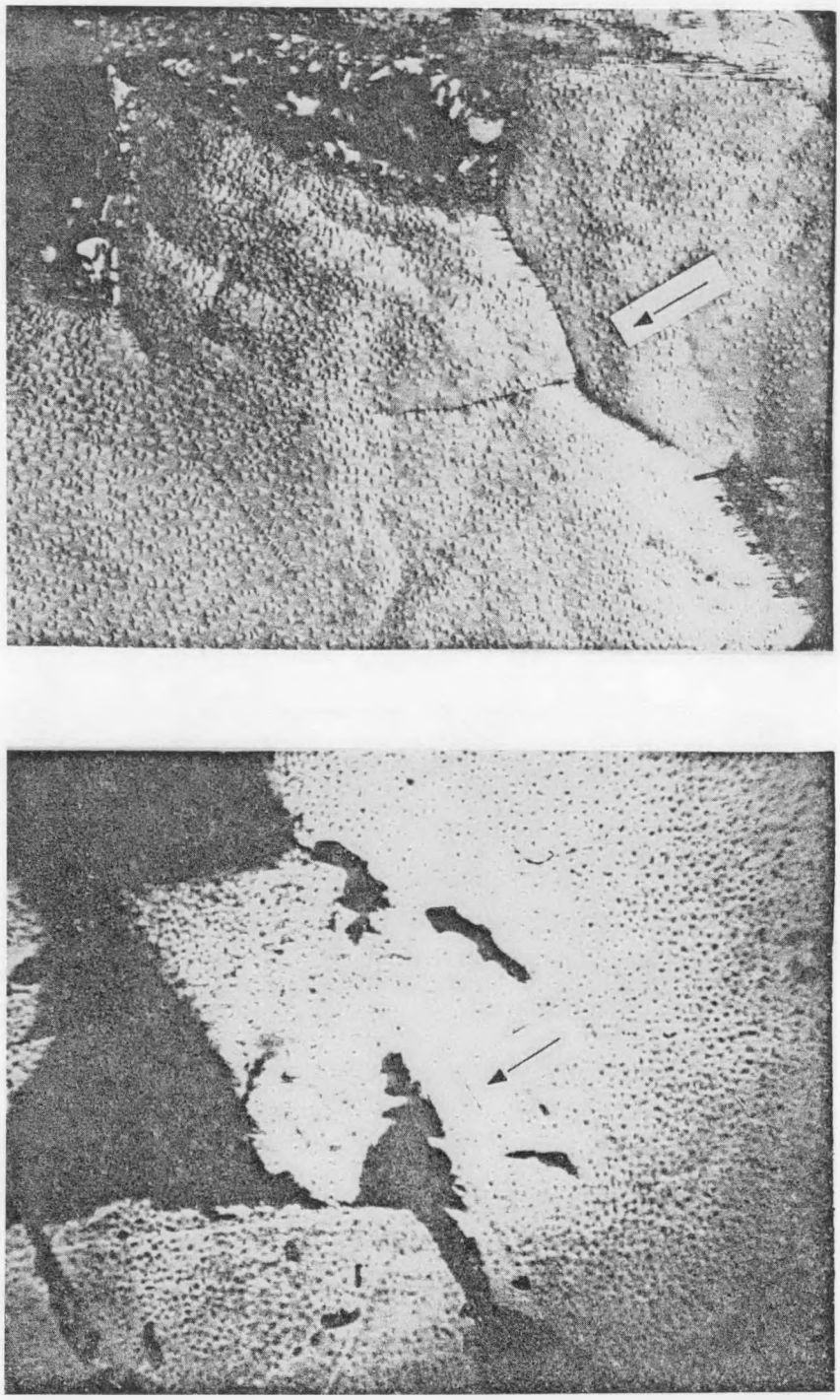

Fig. 22. Surface morphology associated with a buried inclusion (#3678A). (a) Optical photomicrograph 212X. (b) Infrared transmission photomicrograph 151X.

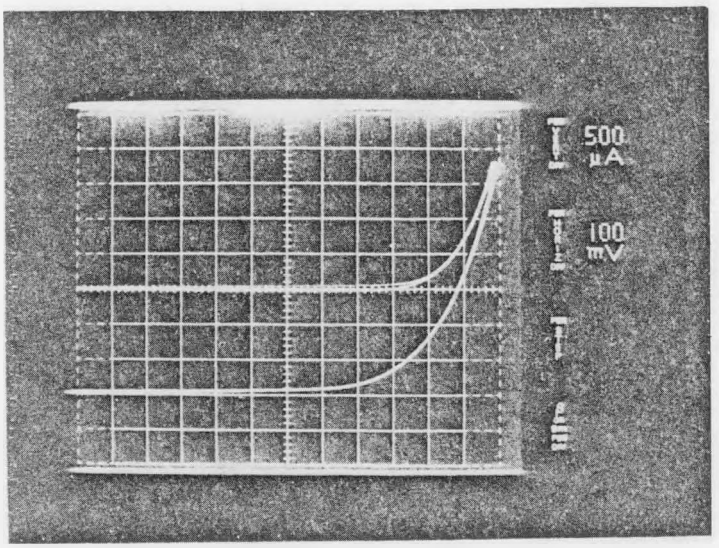

Fig. 23. Surface morphology and I-V curve of a GaAsSb (1.15eV) junction with an area of 0.68 cm^2.

both the n and p layers. Solar cells with a 1.15-eV bandgap have been fabricated and tested. A cross-section is seen in Fig. 24. The maximum quantum efficiency observed to date has been 24%. Again, short diffusion length appears to be the problem.

The use of Zn as a substitute for Mg as the p-type dopant appeared to give identical results. Attempts to use Te as the n-type dopant instead of Sn produced very poor solution wipe-off at the growth conditions used.

Either the dislocation distribution or stoichiometry of the layer could cause the low diffusion lengths. The final layers, after grading, are grown at 770°C, a temperature very near the pseudobinary melting point of $GaAs_{.84}Sb_{.16}$. Under these conditions a larger nonstoichiometric region of the solid is expected than at lower temperatures, and an enhanced incorporation of nonradiative centers and traps could occur. Currently we are investigating lower temperature growth and means of changing dislocation morphology by using different growth techniques and orientations.

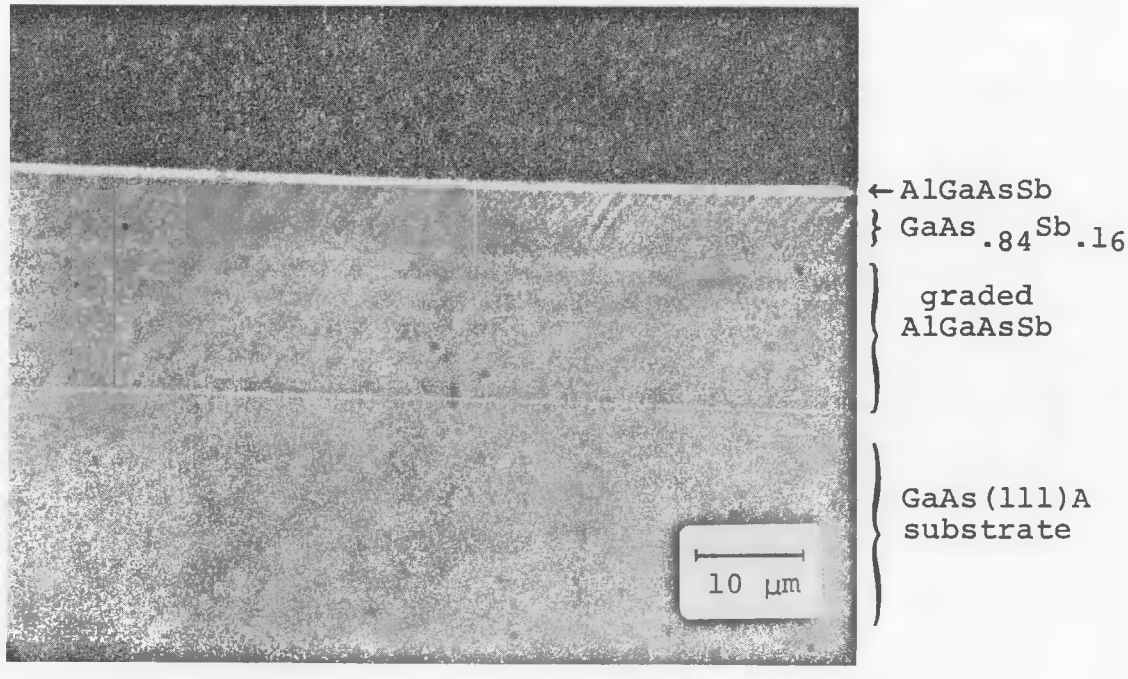

Fig. 24. Cleaved section of a complete low bandgap solar cell Striations at each point of interruption in the graded layer cooling cycle are observed.

9. CONCLUSIONS AND RECOMMENDATIONS

Preliminary investigation into the nature of AlGaAsSb shows this alloy to be applicable to multijunction solar cells. Compositions of the $Al_xGa_{1-x}As_{.84}Sb_{.16}$ with $0 < x < 0.88$ have been grown. This means that the necessary compositions in the direct and indirect bandgap regions can be grown, and that a lattice-matched, two-junction cell with junctions in 1.15-eV and 1.65-eV materials is possible.

Aluminum incorporation in the solid decreases with increasing X^{ℓ}_{Sb} for a constant X^{ℓ}_{Al}. The most rapid decline occurs with the addition of only a few percent Sb. While Sb in the presence of Al goes through a maximum similar to that observed in the ternary alloy.

Continuous lattice grading by LPE from GaAs to $GaAs_{.84}Sb_{.16}$ has been achieved using Al depletion, which in turn reduces As activity. The orientation best suited for continuous grading has been found to be the (111)A surface which exhibited the largest grading thickness compatible with complete solution removal. Although (100) surfaces have a higher growth rate, surface morphology is the poorest observed for the growth conditions used, while (111)B substrates produce the lowest growth rate and a surface structure intermediate between the other two. Growth rate is observed to decrease in the order (100) > (111)A > (111)B.

Surface morphology has been found to improve if growth is performed from a column-V rich solution. The worst surfaces have been observed from stoichiometric melt compositions. Most of this behavior is attributable to variations in As solubility, which is minimum at the stoichiometric composition. From Sb and As rich solutions, the dislocation morphology at Sb/Ga = 2.5 is a cellular structure representing small angle grain boundaries, but at Sb/Ga = 4.0 mismatch dislocations are observed.

Continuous grading by LPE, in this instance, may be limited to a particular temperature region. Addition of Al causes a reduction in X_{As}^{ℓ} that continues to decrease as the temperature is lowered during growth. Most of the experiments on continuous grading have been performed between 830°C and 760°C. Growth much below this temperature has usually produced surfaces with a dull finish. If temperatures below ~ 750°C are required in order to minimize stoichiometric defects, then step grading or VPE methods will need to be utilized, if sufficient As is to be available. This leads to the question of what minimum As concentration is needed to produce good quality epitaxial layers, and whether there is a concentration at which dislocation morphology changes. Determination of a critical concentration may prove useful for other alloy systems when continuous grading techniques are contemplated. Further investigations of this are suggested.

Etch pit studies have shown that inclined dislocation densities on GaAs(111)A continuously-graded layers to be heterogeneously distributed with an average density $\geq 10^6$ cm^{-2}. Most of these are generated during grading, with a substrate containing 10^5 cm^{-2} dislocations contributing about 2 to 3 times more dislocations than a substrate with 10^4 cm^{-2}. This may not be a large factor at the 10^6 cm^{-2} level but this factor may tip the balance from one dislocation distribution to another.

Examination of initial growth islands on a mismatched layer revealed that dislocation bunching may be caused by regions where islands meet. These dislocations are already present at the perimeter of each island before they meet and not just a result of their meeting. This phenomenon has been observed on GaAs (111)A where the substrate surface is also a glide plane. Whether similar behavior is seen on the (111)B where the dislocation core energy is higher or the (100) plane where growth is no longer on a glide surface remains to be investigated.

Because of the fundamental nature of such behavior and its ramifications on many solar cell schemes this area should be actively investigated.

Step grading may change the entire dislocation morphology and some indication of a more even spread has been obtained. A more detailed look at this method is under way and should be continued, particularly since the As solubility is higher in the absence of Al and lower growth temperatures are possible. Whether dislocations bend over at compositional changes of the correct amount remains to be observed. Orientation effects with step grading and the possible use of steady state LPE are recommended.

Solar cell progress is presently slowed because of short diffusion lengths. Whether dislocations acting as recombination centers or other defects caused by nonstoichiometric conditions at growth are the reason is not known at this time. This question is receiving top priority and diffusion length as a function of growth conditions is now being investigated.

Finally, because low leakage large-area junctions have been observed and the proper alloy compositions are attainable within the phase field of the system, further work on this quaternary system is strongly recommended. Since the number of variables such as orientation, temperature, solution composition dopants, and dislocation density to name a few, are substantial, a continued program coupled with another program emphasizing TEM analysis is suggested.

Arsenic availability during growth has been noted as one of the most important parameters. In the event satisfactory growth is unattainable within the range of LPE, then organometallic vapor phase growth should be investigated. As a comparison, LPE $Al_xGa_{1-x}As$ with $x > 0.20$ is seldom grown below

800°C while VPE using organometallics can form $Al_{.90}Ga_{.10}As$ at temperatures < 730°C. Besides the ability to increase As availability the possibility of completely fabricating a stacked solar cell in one deposition is made available. As yet growth of AlGaAsSb by organometallic methods has not been reported and investigation of this approach is recommended.

10. REFERENCES

1. R. E. Nahory, M. A. Pollack, J. C. DeWinter, and K. M. Williams, J. Appl. Phys. 48, 1607 (1977).

2. T. Waho, S. Ogawa, and S. Maruyama, Jap. J. Appl. Phys. 16, 1875 (1977).

3. H. Sakaki, L. L. Chang, R. Ludeke, C. Chang, G. A. Sai-Halasz, and L. Esaki, Appl. Phys. Lett. 31, 211 (1977).

4. E. K. Muller and J. L. Richards, J. Appl. Phys. 35, 1233 (1964).

5. G. A. Antypas and R. L. Moon, J. Electrochem. Soc. 121, 416 (1974).

6. R. L. Moon and J. Kinoshita, J. Cryst. Growth 21, 149 (1974).

7. R. L. Moon, J. Cryst. Growth 27, 62 (1974).

8. R. Ghez and J. S. Lew, J. Cryst. Growth 20, 273 (1973).

9. S. Komiya, K. Akita, Y. Nishitani, S. Izosumi, and T. Kotani, J. Appl. Phys. 47, 3367 (1976).

10. J. W. Matthews in Epitaxial Growth, ed., J. W. Matthews (Academic Press, 1975), p. 559.

11. M. Shindo, S. Mukai, and S. Gonda; Jap. J. Appl. Phys. 16, 1485 (1977).

12. M. Panish, J. Appl. Phys. 44, 2667 (1973).

13. C. S. Kang and P. E. Greene in Proc. 1968 Symposium on GaAs (IPPS, London, 1969), p. 18.

*U.S. GOVERNMENT PRINTING OFFICE: 1979-640-092/ 1131